P516758.PDF [Page: 3 of 96]

DEFENCE R&D DÉFENSE

A Review of Literature: Experimental and Computational Investigation of Fatigue Crack Propagation in Stiffened Plates

Brian Yuen and Farid Taheri

Department of Civil Engineering
Dalhousie University
PO Box 1000, Halifax, Nova Scotia, Canada, B3J 2X4

Contract #W7707-008441/001/HAL

Defence R&D Canada

Contractor Report
DREA CR 2001-141
September 2001

National Defence Défense nationale

Canada

P516758.PDF [Page: 4 of 96]

Copy No: _____

A Review of Literature: Experimental and Computational Investigation of Fatigue Crack Propagation in Stiffened Plates

Brian Yuen and Farid Taheri

Department of Civil Engineering
Dalhousie University
PO Box 1000, Halifax, Nova Scotia, Canada, B3J 2X4

Contract No W7707-008441/001/HAL

Defence Research Establishment Atlantic

Contractor Report

DREA CR 2001-141

September 2001

Authors

Brian Yuen

Farid Taheri

Contract Scientific Authority

D.C.Stredulinsky

Approved by

J.L. Kennedy

Head, Warship Signatures & Safety

Approved for release by

Kirk Foster

Chair/DRP

The scientific or technical validity of this Contract Report is entirely the responsibility of the contractor and the contents do not necessarily have the approval or endorsement of Defence R&D Canada.

© Her Majesty the Queen as represented by the Minister of National Defence, 2001

© Sa majesté la reine, représentée par le ministre de la Défense nationale, 2001

P516758.PDF [Page: 6 of 96]

Abstract

This report is a review of the subject of fracture mechanics focusing mainly on its application on stiffened sheet structures. It is written for readers who have some basic knowledge of fracture mechanics in a general sense but are interested in learning more on this specific and complex aspect of the subject. This report has six chapters. Chapter one is an *introduction* that focuses on the application of stiffened sheet structures. Chapter two reviews the fracture mechanics concepts of strain energy release rate, stress intensity factor, crack resistance and residual strength. Chapter three presents the general theories behind dynamic fracture mechanics and the crack arrest process. Chapter four applies the concepts and theories from Chapter two and three to stiffened sheet structures. Factors that can be used in designing these structures and various parameters that affect their performance are described in this chapter. The graphical representations of the crack arrest process in these structures are also presented in this chapter. Chapter five discusses several methods for analyzing and modeling stiffened sheet structures. In particular the analytical method, the finite element method, the boundary element method, and the finite difference method are presented. Results from several investigators demonstrate the effectiveness of each of these methods. Chapter six contains the concluding remarks on this report.

Résumé

Le présent rapport traite de la mécanique des ruptures et principalement de son application aux structures construites en plaques raidies. Il est rédigé à l'intention des lecteurs possédant certaines connaissances de base en mécanique des ruptures en général et intéressés à en apprendre davantage sur cet aspect spécifique et complexe du sujet. Le rapport comprend six chapitres. Le chapitre un est une introduction visant particulièrement l'application des structures en plaques d'acier raidies. Le chapitre deux est un survol des concepts de la mécanique des ruptures que sont le taux de libération d'énergie de déformation, le facteur d'intensité des contraintes, la résistance aux fissures et la résistance résiduelle. Le chapitre trois présente les théories générales sous-jacentes à la dynamique de la mécanique des ruptures et aux processus antifissures. Le chapitre quatre traite de l'application des concepts et des théories présentées aux chapitres deux et trois aux structures en plaques d'acier. Les facteurs utilisables pour concevoir ces structures et les divers paramètres pouvant affecter leur performance sont décrits dans ce chapitre. Les représentations graphiques des processus antifissures de ces structures sont également présentées dans ce chapitre. Le chapitre cinq traite de diverses méthodes d'analyse et de modelage des structures en plaques d'acier raidies. Les méthodes analytique, d'analyse par éléments finis, par éléments de contour, et des différences finies sont présentées. Les résultats de diverses enquêtes démontrent l'efficacité de chacune de ces méthodes. Le chapitre six est la conclusion du rapport.

P516758.PDF [Page 7 of 96]

This page intentionally left blank.

P516758.PDF [Page: 8 of 96]

Executive summary

Background:

The Warship Signatures and Safety (WSS) Section at DREA has been developing and testing methods for application of realistic sea loads to finite element models to predict hull structural performance. Much of this work has been incorporated into a Defence Research and Development Canada major project entitled "Improved Ship Structural Maintenance Management" (ISSMM). One component of this work is the assessment of the behavior of fatigue cracks in ship structures. There are several fatigue crack propagation models available, each taking a different approach to model fatigue loading and the associated propagation. Selection of the most suitable model for the assessment of ship fatigue crack propagation (FCP) is still challenging and can be quite complex, partly because wave loading is semi-random. Contracted work to Dalhousie University has provided an in depth survey of available FCP models and fatigue test methods, and has examined in detail nineteen FCP models. The work has also included an experimental fatigue crack propagation testing program, subjecting several center-cracked specimens of 350 WT steel (used in the Halifax class frigates) to both constant amplitude loading and semi-random loading. The initial work concentrated on unstiffened plates. Ship structures normally employ stiffened panels. Ongoing work at Dalhousie University is extending the research to consider the effect of stiffeners on crack propagation.

Principal Results:

The principal result of this phase of the work has been to conduct a literature review on the application of fracture mechanics to propagation of cracks in stiffened panels. The report considers related fracture mechanics theory, and various analytical and numerical methods for modeling crack propagation in stiffened structures.

Significance of Results:

This investigation should help provide better crack propagation prediction tools in the ISSMM software.

Yuen, B., Taheri F. 2001. A Review of Literature: Experimental and Computational Investigation of Fatigue Crack Propagation in Stiffened Plates. DREA CR 2001-141 Defence Research Establishment Atlantic.

P516758.PDF [Page: 9 of 96]

Sommaire

Explication:

La section Warship Signatures and Safety (WSS – sécurité et signature des navires de guerre) du CRDA a développé et testé des méthodes pour l'application de charges d'eau réalistes à des modèles d'éléments finis pour prédire les performances structurales des coques. La majeure partie des travaux ont été incorporés dans un grand projet de Recherche et développement en matière de défense Canada appelé « Gestion améliorée de la maintenance de la structure des navires » (GAMSN). Une partie des travaux consiste à évaluer le comportement des fissures de fatigue dans les structures de navire. Divers modèles de propagation des fissures de fatigue existent, chacune empruntant une approche différente pour modeler la charge de fatigue et la propagation associée. La sélection des modèles les plus appropriés pour évaluer la propagation des fissures par fatigue (PFF) est encore difficile et peut être très compliquée, en partie du fait que les charges de vague sont semi-aléatoires. Les travaux effectués à l'université de Dalhousie ont permis d'étudier en profondeur des modèles de PFF disponibles et des méthodes d'essai de fissures, et d'examiner en détail 19 modèles de PFF. Les travaux englobent également un programme d'essai expérimental de propagation de fissures de fatigue dans lequel divers spécimens en acier 350 WT fissurés au centre (utilisé pour les frégates de la classe Halifax) sont soumis à des charges d'amplitude constante et semi-aléatoires. Les premiers travaux ont porté surtout sur les plaques non raidies. Des plaques raidies sont habituellement utilisées pour les structures de navire. Les travaux effectués à l'Université de Dalhousie poussent la recherche plus loin en étudiant l'effet des raidisseurs sur la propagation des fissures.

Principaux résultats:

Les principaux résultats obtenus lors de cette phase des travaux ont permis d'effectuer un survol de la littérature traitant de l'application de la mécanique des ruptures dans la propagation des fissures dans les plaques raidies. Le rapport présente la théorie de la mécanique des ruptures connexes et diverses méthodes analytiques et numériques pour simuler la propagation de fissures dans des structures raidies.

Importance des résultats:

L'étude contribuera à fournir de meilleurs outils de prédiction de propagation des fissures pour le logiciel GAMSN.

Yuen, B., Taheri F. 2001. A Review of Literature: Experimental and Computational Investigation of Fatigue Crack Propagation in Stiffened Plates. CRDA CR 2001-141 Centre pour la Recherche de la D'efence Atlantique.

P516758.PDF [Page: 16 of 96]

Table of Contents

ABSTRACT i

EXECUTIVE SUMMARY iii

TABLE OF CONTENTS v

LIST OF FIGURES vii

1 INTRODUCTION 1

2 SOME BASIC CONCEPTS 2

2.1 Introduction 2
2.2 Strain Energy Release Rate 2
2.3 Stress Intensity Factor 3
2.4 Crack Resistance 5
2.5 Residual Strength 8

3 DYNAMICS AND CRACK ARREST 10

3.1 Introduction 10
3.2 Crack Speed and Kinetic Energy 10
3.3 Crack Arrest Principles 12

4 STIFFENED SHEET STRUCTURES 15

4.1 Introduction 15
4.2 Design Factors for Stiffened Structures 16
4.2.1 Stress Intensity Modification Factor 16
4.2.2 Stiffener Efficiency Factor 18
4.2.3 Load Concentration Factor 19
4.2.4 Method of Estimation 21
4.3 R Curve of Stiffened Panel 22
4.4 Residual Strength of Stiffened Panel 25
4.5 Crack Arrest Parameters 28
4.5.1 Dynamic Effects 28
4.5.2 Integral and Welded Stiffeners 29
4.5.3 Stiffener Yielding 29
4.5.4 Broken Stiffener 30
4.5.5 Fastener Failure 32

5 METHODS OF ANALYSIS 34

5.1 Introduction 34
5.2 Analytical Methods 34
5.2.1 Vlieger and Poe's Method 35
5.2.2 Crichlow's Method 36
5.2.3 Mixed Mode Loading Analysis 38
5.2.4 Multiple Cracks Analysis 42
5.3 Finite Element Method 46
5.3.1 Shear Element 46
5.3.2 Higher Order Element 51
5.4 Boundary Element Method 56
5.4.1 Application to Cracked Stiffened Panels 58
5.4.2 Dynamic Effects of Breaking Stiffeners 62
5.5 Finite Difference Method 68

P516758.PDF [Page: 11 of 96]

5.5.1 *Basic Equations in Dynamic Fracture Analysis* 68
5.5.2 *Analysis by Liu et al* 70
5.5.3 *Analysis by Wang et al* 72

6 SUMMARY 78

REFERENCES 79

PS16758.PDF [Page: 12 of 96]

List of Figures

FIGURE 1-1 CROSS SECTION OF SHIP HULL [6] 1
FIGURE 2-1 LOADING ON A CRACKED PLATE AND THE RESULTING LOAD-DISPLACEMENT DIAGRAM [2] 3
FIGURE 2-2 STATE OF STRESS AT CRACK TIP [2] 5
FIGURE 2-3 R CURVE UNDER PLANE STRAIN [2] 5
FIGURE 2-4 R CURVE UNDER PLANE STRESS [2] 7
FIGURE 2-5 RESIDUAL STRENGTH DIAGRAM OF THREE METALS [2] 8
FIGURE 2-6 METHOD OF FEDDERSEN [2, MODIFIED] 9
FIGURE 3-1 REPRESENTATION OF KINETIC ENERGY [2] 11
FIGURE 3-2 CRACK ARREST DUE TO DECREASING G [2] 12
FIGURE 3-3 EFFECT OF CRACK SIZE ON G_{arrest} [2] 13
FIGURE 3-4 ARREST DUE TO RISTING R [2] 13
FIGURE 3-5 WELDED CRACK-ARREST INSERT [2] A: ARREST, B: ARREST NOT ACHIEVED 14
FIGURE 4-1 THROUGH-THE-THICKNESS CRACK IN A SKIN-STIFFENED PANEL [6] 15
FIGURE 4-2 STRESS INTENSITY MODIFICATION FACTORS FOR A ONE-BAY CRACK CENTRED BETWEEN TWO STIFFENERS [6] 18
FIGURE 4-3 STIFFENER EFFICIENCY FACTOR FOR A ONE-BAY CRACK [6] 19
FIGURE 4-4 STIFFENER LOAD CONCENTRATION FACTOR IN MOST HIGHLY LOADED STIFFENER [6] 20
FIGURE 4-5 RIVET FORCES IN MOST HIGHLY LOADED RIVETS [6] 21
FIGURE 4-6 BOLTED ARREST STRIPS [2] 23
FIGURE 4-7 R CURVE CONCEPT FOR STIFFENED PANEL (CRACK EXTENDING TO STRINGER) [2] 24
FIGURE 4-8 R CURVE CONCEPT FOR STIFFENED PANEL (SHORT CRACK) [2, MODIFIED] 25
FIGURE 4-9 RESIDUAL STRENGTH DIAGRAM OF STIFFENED PANEL [3, MODIFIED] 26
FIGURE 4-10 EFFECT OF STRINGER ON RESIDUAL STRENGTH DIAGRAM (A) STRINGER CRITICAL, (B) PLATE CRITICAL [3, MODIFIED] 27
FIGURE 4-11 STIFFENER PLASTIC DEFORMATION [3] 28
FIGURE 4-12 EFFECTS OF APPLIED STRESS LEVELS ON THE STIFFENER EFFICIENCY [6] 30
FIGURE 4-13 STIFFENER EFFICIENCY FACTOR FOR A TWO-BAY CRACK WITH A CENTRE BROKEN STIFFENER [6] 31
FIGURE 4-14 EFFECT OF BROKEN STIFFENER ON STRESS INTENSITY FACTOR [6] 31
FIGURE 4-15 RESIDUAL STRENGTH DIAGRAM FOR A PANEL WITH THREE STRINGERS AND A CENTRAL CRACK [2] 32
FIGURE 4-16 CRITERION FOR FASTENER FAILURE [2] 33
FIGURE 5-1 ANALYTICAL SOLUTION FOR STIFFENED SHEET [2] 35
FIGURE 5-2 EFFECTIVE WIDTH CONCEPT [2] 37
FIGURE 5-3 SYMMETRICALLY CRACK-STIFFENED RECTANGULAR PANEL UNDER MIXED MODE LOADING [12] 39
FIGURE 5-4 MODE I PART OF LOADING AND ITS BREAK-UP [12] 39
FIGURE 5-5 MODE II PART OF LOADING AND ITS BREAK-UP [12] 40
FIGURE 5-6 VARIATION OF STRESS INTENSITY FACTOR WITH STIFFENER LOCATION FOR MODE I PROBLEM [12] 42
FIGURE 5-7 MODEL OF A MULTIPLE CRACKED SHEET ATTACHED WITH RIVETED STIFFENERS [8] 42
FIGURE 5-8 THREE CASES FOR SKIN DISPLACEMENT [8] 43
FIGURE 5-9 TWO NUMERICAL EXAMPLES [8] 45
FIGURE 5-10 VARIATION OF STRESS INTENSITY FACTOR WITH RELATIVE CRACK LENGTH [8] 45
FIGURE 5-11 VARIATION OF MUTUAL INTERACTION FACTOR WITH CRACK LENGTH [8] 46
FIGURE 5-12 (A) STIFFENER-ADHESIVE-SHEET COMPOSITE ELEMENT, (B) VARIATION OF SHEAR STRESSES ALONG THE THICKNESS DIRECTION, (C), (D) AND (E) BREAK-UP OF THE COMPOSITE ELEMENT SHOWN IN (A) [13] 47
FIGURE 5-13 FORCES AND DISPLACEMENTS ASSOCIATED WITH CRACK CLOSURE INTEGRAL [13] 49
FIGURE 5-14 EDGE CRACK-STIFFENED PANEL UNDER MODE I LOADING [13] 50
FIGURE 5-15 VARIATION OF TRANSVERSE SHEAR STRESS ALONG STIFFENER CENTRE LINE FOR THE CENTRE CRACK PROBLEM UNDER MODE I LOADING [13] 51

P516758.PDF [Page: 13 of 96]

FIGURE 5-16 (A) SHEET-STIFFENER ARRANGEMENT AND SHEAR STRESS DISTRIBUTION IN THE THICKNESS DIRECTION (B) OVERLAY OF TWO ELEMENTS (C) EQUIVALENT SHEAR STRESS DISTRIBUTION AND OVERLAY ARRANGEMENT [7] 52
FIGURE 5-17 COMPARISON OF VARIATION OF τ_{xz} ALONG THE STIFFENER CENTRE LINE IN THE MODE I PROBLEM [7] 54
FIGURE 5-18 THREE EDGE CRACK LOADING CASES ANALYZED (A) UNIAXIAL LOAD (B) POINT LOAD (C) EQUIBIAXIAL LOAD [7] 55
FIGURE 5-19 VARIATION OF $(\sigma_{ij})_{MAX}/(\sigma_{ij})_{MAX_0}$ WITH STIFFENER LOCATION X_0 FOR EQUIBIAXIAL LOADING [7] 56
FIGURE 5-20 VARIATION OF $(\sigma_{ij})_{MAX}/(\sigma_{ij})_{MAX_0}$ WITH STIFFENER ORIENTATION α FOR EQUIBIAXIAL LOADING [7] 56
FIGURE 5-21 REFERENCE BOUNDARY CONDITIONS FOR A BOUNDARY INTEGRAL ELEMENT PROBLEM [1] 57
FIGURE 5-22 ISOLATED STIFFENER SUBJECTED TO A SET OF IN-PLANE LOADS [11] 60
FIGURE 5-23 CRACKED PANEL REINFORCED BY RIVETED STIFFENERS [11] 61
FIGURE 5-24 BOUNDARY ELEMENT MESH AND CRACK PATHS AFTER TEN CRACK INCREMENTS [11] 62
FIGURE 5-25 CRACK GROWTH DIAGRAM [11] 62
FIGURE 5-26 BROKEN STIFFENER EQUALS UNBROKEN STIFFENER PLUS "OPENING" FORCE P' [9] 63
FIGURE 5-27 PRESSURE DISTRIBUTION ON HALF THE CRACK [9] 64
FIGURE 5-28 BOUNDARY ELEMENT MODEL OF CRACK CONFIGURATION [9] 64
FIGURE 5-29 DYNAMIC STRESS INTENSITY FACTORS FOR VARIOUS CRACK-FACE LOADINGS [9] 65
FIGURE 5-30 STATIC AND PEAK DYNAMIC STRESS INTENSITY FACTORS FOR A CRACK IN A STIFFENED SHEET [9] 67
FIGURE 5-31 DYNAMIC OVERSHOOT OF THE STRESS INTENSITY FACTOR AFTER A STIFFENER BREAKS [9] 67
FIGURE 5-32 RESOLUTION OF A STIFFENED PANEL [5] 71
FIGURE 5-33 CALCULATION MESH FOR QUARTER OF PANEL [5] 71
FIGURE 5-34 COMPARISON OF CRACK VELOCITY [5] 72
FIGURE 5-35 INFLUENCE OF E_s, E ON VELOCITY [5] 72
FIGURE 5-36 A STIFFENED PANEL WITH AN EDGE CRACK [14] 73
FIGURE 5-37 CALCULATION MESH FOR HALF OF PANEL [14] 73
FIGURE 5-38 EQUILIBRIUM OF THE STIFFENER [14] 74
FIGURE 5-39 STATIC K_I VARIATION WITH A_s (X_0 = 0.18 M) [14] 75
FIGURE 5-40 CRACK PROPAGATION WITH DIFFERENT A_s (X_0 = 0.18 M) [14] 76
FIGURE 5-41 STATIC K_I VARIATION WITH X_0 (A_s = 0.2 X 10^{-3} M^2) [14] 76
FIGURE 5-42 CRACK PROPAGATION WITH DIFFERENT X_0 (A_s = 0.2 X 10^{-3} M^2) [14] 77

P516758.PDF [Page: 14 of 96]

1 Introduction

Stiffened sheet structures are metal sheets reinforced by stringers that can be bonded or welded to the sheets, connected to them by fasteners such as rivets or bolts, or machined as an integral part of the panels They are widely used in aircraft, ships and chemical industry structures for their light weight and high resistance They are mostly found in the airframes, fuselages and wings of aircraft and the deck and side plating on a ship as shown in Figure 1 1, where the amount of fatigue loading is the greatest In a static point of view, stiffened structures provide higher buckling strength and flexural stiffness In terms of fracture mechanics, the stringers (or stiffeners) provide a secondary structure for the load to bypass a cracked panel The crack tip stress intensity factor is lowered in the vicinity of an intact stringer so that the growth of a crack towards a stringer is slowed down or even arrested For this reason, a stringer is sometimes called a crack arrester Because of its crack arresting capability, a stiffened structure can sustain cracks safely until it is repaired or its economic service life has expired Such structure is said to have high damage tolerant and it can represent major cost savings as the inspection interval of the structure for cracks can be longer The rest of this report seeks to provide the reader some methods of predicting the fracture behaviour of stiffened sheet structures such that their damage tolerant advantage can be taken to the fullest

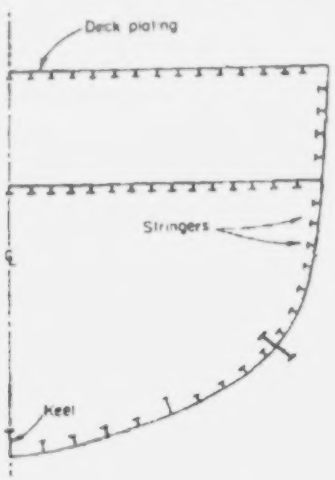

Figure 1-1 Cross section of ship hull [6]

P516758.PDF [Page: 15 of 96]

2 Some Basic Concepts

2.1 Introduction

This chapter gives the reader a brief introduction to some basic concepts in fracture mechanics that is relevant to this report Readers who are familiar with Griffith's fracture criterion and the concepts of strain energy release rate and stress intensity factor should find this chapter a helpful review Understanding of the last two sections of this chapter on crack resistance and residual strength is essential for the next two chapters In particular the G curve and R curve presented in the crack resistance section provide a graphical representation of the fracture criterion They are also the basis of dynamic fracture mechanics and crack arrest that are discussed in the next chapter On the other hand, the residual strength diagram is a convenient tool in determining the fracture strength in a stiffened structure, which is discussed in Chapter 4

2.2 Strain Energy Release Rate

In 1921, Griffith [2] proposed an energy criterion for fracture based on the energy conservation law which can be stated as crack growth can occur if the energy required to form an additional crack of size da can just be delivered by the system The energy delivered by the system comes in forms of the release of the strain energy in the system and the work done by the external load on the system The strain energy of a deformed body can be determined as the area under its load-displacement curve as shown in Figure 2-1 For a plate of unit thickness the Griffith energy criterion can be written in terms of the strain energy and the external work as

$$\frac{d}{da}(U - F + W) = 0 \quad \text{or} \quad \frac{d}{da}(F - U) = \frac{dW}{da} \tag{2-1}$$

where U is the strain energy contained in the plate, F is the work performed by the external force and W is the energy for crack formation The "strain energy release rate" or the "crack extension force" is then defined as $G = d(F-U)/da$, and the crack resistance (force) $R = dW/da$ Although G and R are called forces, it should be noted that they are energy measurements and have the unit of energy per unit crack extension and per unit

P516758 PDF [Page: 16 of 96]

thickness At fracture $G = G_c$, where G_c is known as the critical strain energy release rate The value G_c depends on the specimen thickness but is a material constant under plane strain condition

For mode I loading on a cracked plate, in which the load is perpendicular to the crack surfaces, the strain energy release rate can be shown to be equal to

$$G_I = \frac{\pi\sigma^2 a}{E} \tag{2-2}$$

where G_I is the mode I strain energy release rate, σ is the far-field applied stress, a is the length of an edge crack or half the length of a central crack, and E is the modulus of elasticity of the plate Similar equations exist for the other loading modes (sliding mode and tearing mode) and the total energy release rate in combined mode cracking is obtained by adding the energies from the different modes It should be noted that the main focus of this report is on mode I loading and G denotes the mode I strain energy release rate

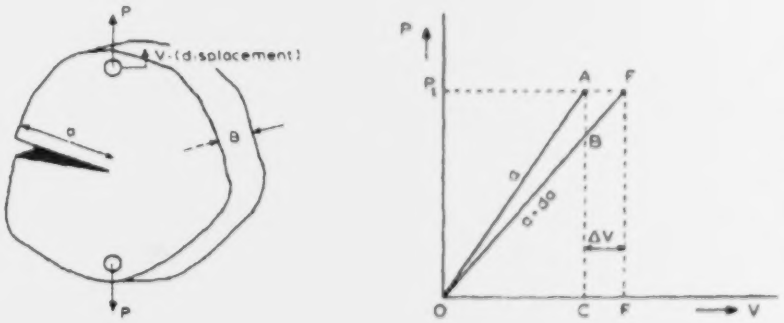

Figure 2-1 Loading on a cracked plate and the resulting load-displacement diagram [2]

2.3 *Stress Intensity Factor*

Although the fracture criterion is based on energy equilibrium, a stress-based fracture parameter called the stress intensity factor, K, is more commonly used in experimental and numerical analysis The stress intensity factor is a measure of the severity of the crack in terms of the far-field applied stress, crack size, and specimen geometry The crack tip stresses are proportional to the stress intensity factor, as shown

P516758.PDF [Page: 17 of 96]

in Equations 2-3 that are derived from the Westergaard [2] complex stress function. For mode I loading:

$$\begin{aligned}
\sigma_x &= \frac{K_I}{\sqrt{2\pi r}}\cos\frac{\theta}{2}\left[1-\sin\frac{\theta}{2}\sin\frac{3\theta}{2}+\ldots\right] \\
\sigma_y &= \frac{K_I}{\sqrt{2\pi r}}\cos\frac{\theta}{2}\left[1+\sin\frac{\theta}{2}\sin\frac{3\theta}{2}+\ldots\right] \\
\tau_{xy} &= \frac{K_I}{\sqrt{2\pi r}}\cos\frac{\theta}{2}\sin\frac{\theta}{2}\sin\frac{3\theta}{2}\ldots \\
\sigma_z &= 0 \quad \text{(plane stress)} \\
\sigma_z &= \nu(\sigma_x+\sigma_y) \quad \text{(plane strain)}
\end{aligned} \tag{2-3}$$

In Equation 2-3, K_I denotes the mode I stress intensity factor, ν is the Poisson ratio, and r and θ are as defined in Figure 2-2. K_I is turn given by the following:

$$K_I = Y\sigma\sqrt{\pi a} \tag{2-4}$$

where σ and a are as defined in Equation 2-2 and Y is a dimensionless geometric parameter that depends on crack length of specimen width ratio, specimen width to length ratio, etc. The values for Y for much common geometry are available in various design handbooks. For an infinite panel, Y is equal to 1.

Similar to the strain energy release rate, the fracture condition in terms of the stress intensity factor can be written as $K = K_c$ where K_c is the critical stress intensity factor. K_c is also a material constant under plane strain condition and it can be shown that G and K are related by the following equations (subscripts indicate mode I loading):

$$\begin{aligned}
G_I &= \frac{K_I^2}{E} \quad \text{(plane stress)} \\
G_I &= (1-\nu^2)\frac{K_I^2}{E} \quad \text{(plane strain)}
\end{aligned} \tag{2-5}$$

Both G_c and K_c are measures of fracture toughness of a material and it can be seen that the stress criterion for fracture is the same as the energy criterion discussed in the previous section.

P516758.PDF [Page: 18 of 96]

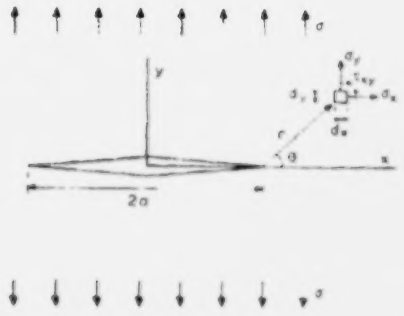

Figure 2-2 State of stress at crack tip [2]

2.4 *Crack Resistance*

It is stated in the last sections that fracture can occur when the strain energy release rate is equal to the critical value required for crack growth For a truly brittle material like glass, this value is the energy required to form the new free surfaces This means the crack resistance is independent of crack length, R = constant G_c The situation in a ductile material like a metal is different In addition to surface energy, in metals plastic deformation occurs in front of the crack due to high stress concentration and during crack extension energy is expended by the formation of a new plastic zone at the tip of the advanced crack Experimentally, it appears that this plastic energy is approximately the same for every crack increment for plane strain cracks or when the material toughness is low When the toughness is high, the R increases more steeply This means under plane strain R is represented by a straight horizontal line $R = G_{Ic}$ when it is plotted against crack length. This is shown in Figure 2-3 where G_{Ic} is the critical strain release rate for the case of mode I loading and plane strain condition

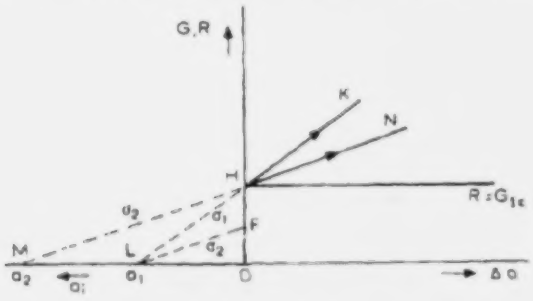

Figure 2-3 *R* curve under plane strain [2]

Figure 2-3 is a universal representation of the fracture criterion The crack extension Δa is plotted on the right and the initial crack size a_i is on the left. Energy is plotted on the vertical axis For plane strain condition, R is constant and is plotted as a straight horizontal line $R = G_{Ic}$ This represents the energy required for fracture, or simply called an R curve According to Equation 2-5, for a particular stress σ the energy release rate G is directly proportional to the crack size a Thus G is represented by a straight line with a slope that is proportional to σ^2 These are shown in Figure 2-3 as lines LF and MHN at a stress of σ_2 and line LHK at a stress of σ_1 where $\sigma_1 > \sigma_2$ Note that line LHK has a steeper slope as a result of greater stress The fracture criterion can then be interpreted from the graph as follows By loading the crack a_1 from zero stress to σ_1, its G value increases from O to F. Fracture does not occur since F < G_{Ic}. Further increase of the stress to σ_2 raises G to the point H Then fracture occurs as $G = G_{Ic}$ and remains greater than G_{Ic} as the crack grows For larger initial crack size at a_2, G_{Ic} is reached (and thus fracture occurs) at a lower stress of σ_2 Note that LF and MHK are parallel since they are at the same stress

It should be noted that G is a straight line only for an infinite plate containing a crack For any other loading conditions or specimen geometry, G would increase or decrease during crack growth For example, at the onset of crack extension, G values are the same in the cracked plate under constant stress and under fixed grips However, during crack growth the stress drops under fixed grip conditions, resulting in a decreasing G curve that curves downwards Furthermore, for a cracked finite panel, the finite width correction can be applied to G that results in a G curve that curves upward instead of straight For a small crack the width correction can be neglected and the G curve is approximately straight For longer cracks the curvature becomes larger and larger The implication of the shape of the G curve on crack arrest is presented in the next chapter

The R curve for plane strain condition has been discussed In reality, the fracture of thin structures such as ship plates occurs between plane strain and plane stress condition In case of plane stress the crack resistance has been shown by experiments to vary with the amount of crack growth Thin plates under plane stress show a steep, rising R curve as shown in Figure 2-4 The R curve starts at zero since the energy required for crack initiation by growth and coalescence of microvoids is presumably small in

comparison with the plastic energy for crack growth in a ductile material This means crack growth occurs at any stress different from zero However crack growth does not occur until G reaches a value of B as shown in Figure 2-4 This illustrates an important point about the energy criterion The energy criterion is a necessary condition for crack growth, but not a sufficient condition Crack growth does not occur until the stresses and strains at the crack tip are high enough such that the material is ready to separate

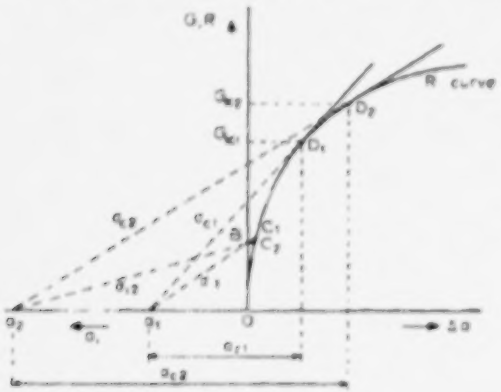

Figure 2-4 *R* curve under plane stress [2]

According to Figure 2-4, a crack of initial size a_1 reaches a G value of B at a stress of σ_{f1} At this point the crack is suddenly extended until G reaches C_1 Further crack growth does not occur after C_1 at stress σ_{f1} since $G < R$ at stress σ_{f1} after C_1 This first discrete crack extension is called pop-in, because it is a sudden metastable crack extension, which is often associated with an audible click Further increase in stress is required for further crack growth along the R curve until $G = G_{Ic1} = D_1$ At point D_1, G remains larger than R as Δa increases Thus final fracture occurs at D_1 At this point the G curve is tangent to the R curve The criterion for fracture under plane stress can then be written as

$$\frac{\partial G}{\partial a} = \frac{\partial R}{\partial a}, \quad G = R \tag{2-6}$$

In summary there is a constant critical strain energy release rate G_{Ic} under plane strain. Rapid fracture occurs when this value is reached In contrast, G_{Ic} under plane stress depends upon crack size and is larger for larger cracks This can be seen in Figure

2-4 where an initial crack size of a_{i2} fails at a higher G_{1c} at D_2. There is also a period of slow crack growth under plane stress after $G = G_{1c}$. This is followed by rapid fracture at $G = G_{1c}$. It should be emphasized that this period of crack growth occurs as the applied stress approaches the fracture stress and should not be confused with crack growth during normal service loading caused by e.g. fatigue or stress corrosion.

2.5 *Residual Strength*

The strength of a material is the highest when no flaws are presence in the material. However due to stress concentration the presence of crack in a material decreases its strength. The strength of a cracked material is called its residual strength, σ_c, and it decreases progressively with increasing crack size. Fracture can occur if the residual strength is exceeded. Therefore a structure that is initially safe under normal service load may be susceptible to fracture in the long run as cracks may initiate and grow in the structure to the size that makes the residual strength equal to the normal service load. Such a crack is said to have reached a critical size and the structure should be repaired or replaced before the crack becomes critical. A residual strength diagram is a plot of the residual strength of a material against the crack length. The critical crack size for a certain service load can then be determined from this diagram. Knowing the fracture toughness of a material, K_c, its residual strength diagram can be obtained from Equation 2-4, namely $\sigma_c = K_c / \sqrt{\pi a}$ with $Y = 1$ for simplicity. This has been done for three metals as shown in Figure 2-5. Clearly the material with the highest fracture toughness has the highest residual strength.

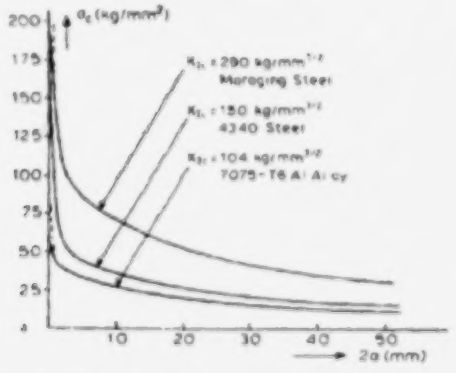

Figure 2-5 Residual strength diagram of three metals [2]

Although the residual strength diagram in Figure 2-5 is simple to construct, it suffers from two deficiencies First, the residual strength of a material should approach the ultimate fracture strength of the material as the crack length, a, approaches zero, not to infinity as suggested by the equation Second, for a finite panel, the residual strength should approach zero as the crack length approaches the width of the panel, W To better represent the realistic behaviour, Feddersen [6] has proposed a technique that is based on displaying test data The technique calls for drawing a straight line from the point $\sigma_c = \sigma_{ys}$, the yield stress of the material, tangent to a point on the curve based on the equation Another tangent line is drawn from the point $2a = W$ to the curve. It turns out that the tangent lines intersect the curve at $\sigma_c = 2/3\sigma_{ys}$ and $2a = W/3$ as shown in Figure 2-6 The residual strength diagram for an unstiffened panel can be constructed in this manner and provides a basis for the stiffened residual strength diagram This is discussed in more detail in Chapter 4

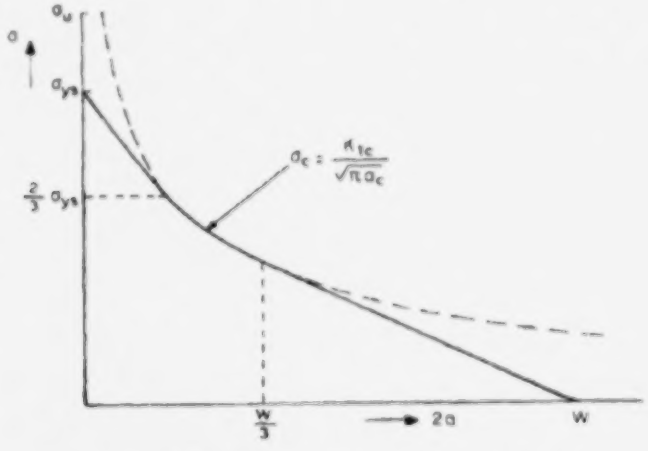

Figure 2-6 Method of Feddersen [2, modified]

3 Dynamics and Crack Arrest

3.1 Introduction

In the previous chapter the concepts of strain energy release rate, stress intensity factor, crack resistance, and residual strength are introduced under static conditions However both crack propagation and fracture are dynamic processes where the crack can grow at a high speed This introduces dynamic effects to the problem due to the inertia forces, rate-dependent material behaviour, and reflected stress waves Thus the stress intensity in the dynamic case is different from the static case The kinetic energy of the crack also enters into the energy criterion for fracture Under the right conditions, crack growth or fracture can be stopped This phenomenon is called crack arrest. For this to happen, the speed of the crack must be reduced to zero. This means the kinetic energy has to be dissipated In this chapter, the theory behind dynamic fracture and crack arrest is presented using concept of R curve discussed in the previous chapter

3.2 Crack Speed and Kinetic Energy

Whenever the strain energy release rate G is greater the crack resistance R, there is a surplus of release energy, $(G-R)$, that can be converted into kinetic energy, E_{km} Since kinetic energy is proportional to the square of speed, the surplus energy also governs the speed at which the crack will propagate through the material Consider the situation depicted in Figure 3-1 It shows the plane strain R curve and a cracked body that had been loaded to fracture As the crack grows at fracture stress, G remains larger than R and an increasing amount of surplus energy is available to be converted to kinetic energy as indicated by the shaded area in Figure 3-1 This explains why final fracture is rapid process with the crack growing across the width of body at a high speed If the surplus energy (shaded area in Figure 3-1) is equated to the familiar formula for kinetic energy, $E_{km} = \frac{1}{2}mv^2$, then the crack speed can be expressed as follows

$$v = 0.38 v_s \left(1 - \frac{a_c}{a}\right) \tag{3-1}$$

where v is the crack speed, $v_s = \sqrt{E/\rho}$ is the speed of sound in the material with E and ρ being the Young's modulus and the specific density of the material respectively, and a_c is the critical crack length. Equation 3-1 predicts how the crack growth rate increases from zero at the start of fracture at $a = a_c$, to a limiting velocity of 0.38 v_s when the crack size is large. However measured crack velocities in different materials are well below the theoretical values predicted by Equation 3-1. Reported propagation rates of ductile cracks are even lower. This is due to a number of assumptions that are made in Figure 3-1 that are discussed below.

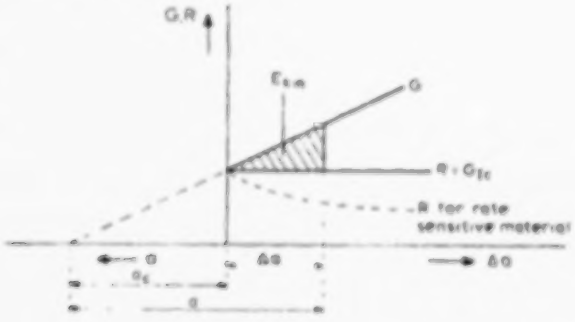

Figure 3-1 Representation of kinetic energy [2]

The case depicted in Figure 3-1 is simplified in a number of ways to facilitate the above discussion. First, the R curve is shown to be a horizontal line. In reality true plane strain condition is rare and in many cases R is a rising function. For a rate sensitive material the R curve may be decaying, as shown in dash in Figure 3-1, since the material behaves in a more brittle manner at higher crack speed. As mentioned in the last chapter, brittle materials do not require plastic energy for crack growth and thus have lower crack resistance. However an increasing crack resistance may also be observed for some materials. Second, in reality the stress distributions in the static and dynamic cases are different, due to the introduction of time dependent parameters. Therefore the strain energy release rate is dependent upon crack speed and the G curve is not a straight line as shown. Recent work on more realistic crack problems has shown that the dynamic stress intensity, and therefore the dynamic strain energy release rate, decreases with increasing crack velocity. The dynamic stress intensity becomes zero when the crack velocity reaches the surface wave velocity. Therefore in real structures, the G and R curves may

P516758.PDF [Page: 25 of 96]

rise and fall as the crack grows depending on the geometry and material properties Crack arrest may result when these curves are crossed The subject of crack arrest is present in the next section

3.3 Crack Arrest Principles

In Figure 3-1 the G curve is depicted as a straight line such that when the fracture stress is reached, G remains greater than R as the crack grows until final failure However, under certain loading conditions or specimen geometry, such as loading a plate with fixed ends or with stiffeners, G decreases with crack length so that crack growth may be arrested Crack propagation and arrest in a stiffened structure, which is the main focus of this report, is discussed in more details in the next chapter The decrease in G may also be a result of the dynamic effects and an example of a decreasing G curve is shown in Figure 3-2 In the figure R is assumed to be constant and G begins to decrease at B At C the condition that $G = R$ is again satisfied However crack arrest does not occur even though $G < R$ from this point onward since the speed of the crack is not equal to zero as the kinetic energy is equal to area ABC The crack slows down after C as the kinetic energy is consumed for further crack growth Crack arrest (crack speed equals zero) finally occurs at E when all the kinetic energy is consumed, such that area CDE = ABC From the figure, one can see that the value of G at arrest is lower than G_{Ic} This lower value is called the arrest toughness It can also be seen from Figure 3-3 that this value depends on the initial crack size, as crack a_{c1} and a_{c2} has different arrest toughness values of G_{I1} and G_{I2} respectively

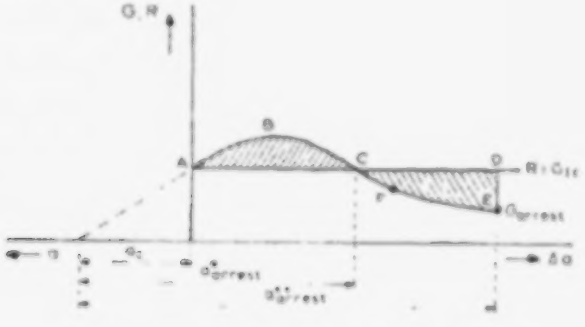

Figure 3-2 Crack arrest due to decreasing G [2]

P516758.PDF [Page: 26 of 96]

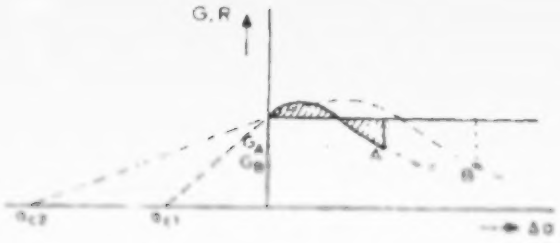

Figure 3-3 Effect of crack size on G_{arrest} [2]

The above discussion on crack arrest illustrates the case when G drops below R. Alternatively crack arrest can occur when R rises above G as depicted in Figure 3-4. R can increase in a number of ways. Due to the growing crack the plastic zone at the crack tip increases in size and through the thickness restraint becomes less. When the plastic zone becomes of a size of the order of the plate thickness, plane stress may develop. As mentioned in the last chapter, this causes a steep rise in R, such that it may become larger than G. Temperature rise in the plastic zone resulting from the high rates of deformation can also cause increase in R. A rise in temperature means that energy is dissipated as heat. This heat energy is supplied from the strain energy release and can be regard as an added crack resistance. The heat generation will depend upon crack speed and the resulting temperature rise will depend upon specimen geometry. Lastly R can be increased by the insertion of strips of material with a higher toughness. This situation is depicted in Figure 3-5. A high toughness strip is welded to the base material and it is shown as a sudden jump in value in the R curve. One can see in Figure 3-5(a) that the kinetic energy can easily be absorbed by the high toughness strip provided that it is wide enough. However the strip is not effective if the crack is too far away from the strip as shown in Figure 3-5(b).

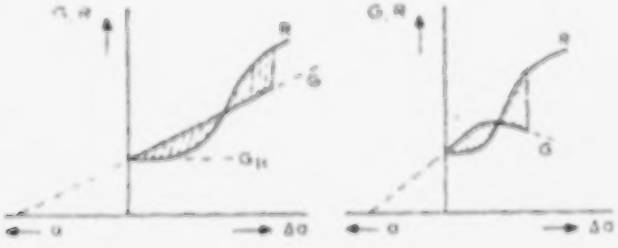

Figure 3-4 Arrest due to rising R [2]

P516758.PDF [Page: 27 of 96]

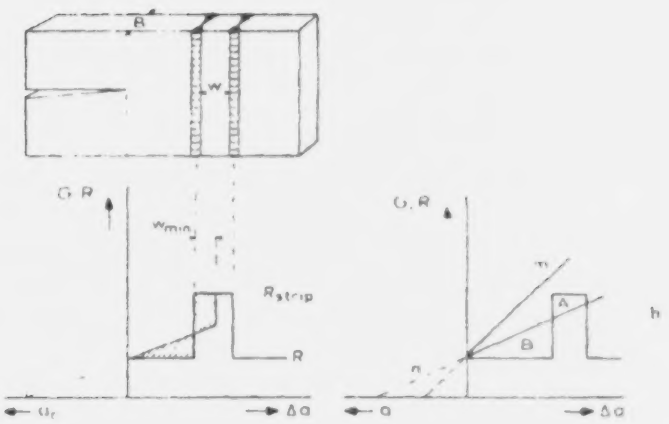

Figure 3-5 Welded crack-arrest insert [2] a. Arrest; b. Arrest not achieved

The above is a simplified discussion on crack arrest which is sufficient for the purpose of this report. The problem, however, is complicated by the following facts First, it is unlikely that the kinetic energy can always be used for crack propagation, particularly in the case of very long cracks for which much of the kinetic energy is contained in a region far behind the crack tip It has been concluded by Maxey *et al* [2] that there is a maximum effective crack length beyond which the crack behaves as if it has a constant size Also, if G drops below G_c, the stresses at the crack tip are also below critical, such that crack growth should be expected to stop even if sufficient kinetic energy is available This is another example illustrating that the energy condition is a necessary condition for crack growth, but it is not necessarily a sufficient condition

P516758.PDF [Page: 28 of 96]

4 Stiffened Sheet Structures

4.1 Introduction

One way to increase the fracture toughness of a structure is to incorporate stiffeners to its structural components. Stiffeners come in all shapes and sizes, ranging from flat straps to the stringers shown in Figure 4-1. Stiffeners can either be mechanically attached by rivets or bolts, welded, or even integral to the component. They exhibit different fracture behaviour, but in all the cases they work by carrying part of the applied load from the skin and thereby reducing the crack tip stress intensity if the skin is cracked. The stress intensity can become so low that crack arrest is possible. The side effect is that the stiffener and fasteners experience higher and higher stress concentration as the crack elongates. When the strengths of the stiffener and fasteners are exceeded, they lose their crack arrest effectiveness. The stiffener and fastener efficiency and load concentration factors can be found in design handbooks and are discussed in this chapter. These factors can be determined by either analytical or numerical methods that are discussed in the next chapter. Also in this chapter is a presentation of the R curve and residual strength concepts as they are applied to stiffened panels. Finally the effects of stiffener and fastener failure are discussed at the conclusion of this chapter.

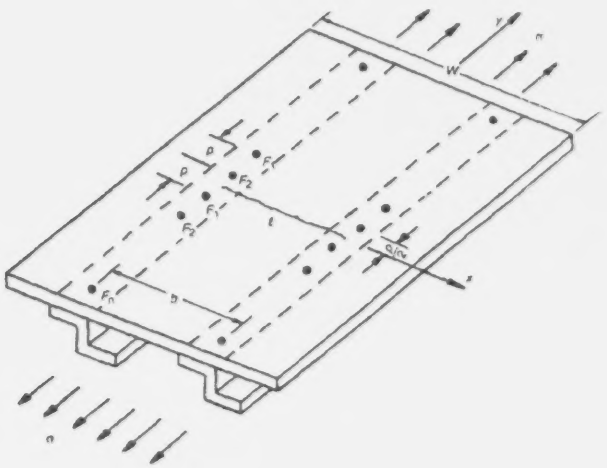

Figure 4-1 Through-the-thickness crack in a skin-stiffened panel [6]

P516758 PDF [Page: 29 of 96]

4.2 Design Factors for Stiffened Structures

This section introduces several factors that can be used to design stiffened structures. They are the stress intensity modification factor, stiffener efficiency factor, and the stiffener and fastener load concentration factors. Their values can be found in various design handbooks for simple geometry. For more complicated arrangements, an analytical or numerical method has to be used, which is discussed in the next chapter. At the end of this section, a method for estimating the load concentration factors with the stress intensity modification factor is presented.

4.2.1 Stress Intensity Modification Factor

Since the stress intensity factor, K, of a stiffened cracked panel is lower than its corresponding unstiffened panel, one way to access the effectiveness of a stiffener is to consider its stress intensity modification factor, C', which is defined as the ratio of the stress intensity factor for the stiffened panel to the stress intensity factor for the plain sheet (without stiffener). Poe [6] has compiled the C' factors for various stiffener configurations in his work and presented them as design graphs. Figure 4-2 is one of the examples, which plot the C' factor against crack length for a one-bay crack in the middle of a bay between two stiffeners. Poe considered the C' factor as a function of attachment spacing (rivet pitch), p, reinforcement spacing, b, and a relative stiffness parameter, μ, which is defined as

$$\mu = \left[1 + \frac{b \cdot t}{A_e} \cdot \frac{E}{E_s}\right]^{-1} \tag{4-1}$$

where t is the sheet thickness, A_e is the effective cross-sectional area of the stiffener, and E and E_s are the Young's modulus for the sheet and the stiffener, respectively. If the stiffener is a stringer, only a part of the stringer (the area that is close to the skin) makes a contribution to reducing the crack tip stress intensity. An estimate for A_e is given as

$$A_e = A\left[1 + \left(\frac{y}{\rho}\right)^2\right]^{-1} \tag{4-2}$$

P516758.PDF [Page: 30 of 96]

where A is the cross-sectional area of the stringer, y is the distance from the inner surface of the sheet to the centroid of the stringer, and ρ is the radius of gyration of the stringer For a flat strap, A_c is approximately equal to the actual size of the strap If the strap is not made of the same material as the sheet, then A_c is modified as

$$A_c = A \cdot F_{ty}f / F_{ty}s \tag{4-3}$$

where F_{ty} and F_{ty} are the tensile yield strength for the stiffener and the sheet respectively In the case of an integral or a welded stiffener, the curves in Figure 4-2 are still applicable by considering very close reinforcement spacing As seen from Figure 4-2, reduction in K increases as relative spacing of the attachment decreases because the smaller the attachment spacing, the more effective load transfer is to the reinforcement However, it turns out the ratio of stiffener modulus to sheet modulus is a more important factor for improving reinforcement efficiency, and thus a higher μ value will result in a greater reduction in K Incorporating the C' factor, the general stress intensity factor in a stiffened structure can be written as

$$K = C'Y\sigma\sqrt{\pi a} \tag{4-4}$$

The strain energy release rate and the residual strength of a stiffened structure can be obtained similarly These are done in the next two sections

P516758.PDF [Page: 31 of 96]

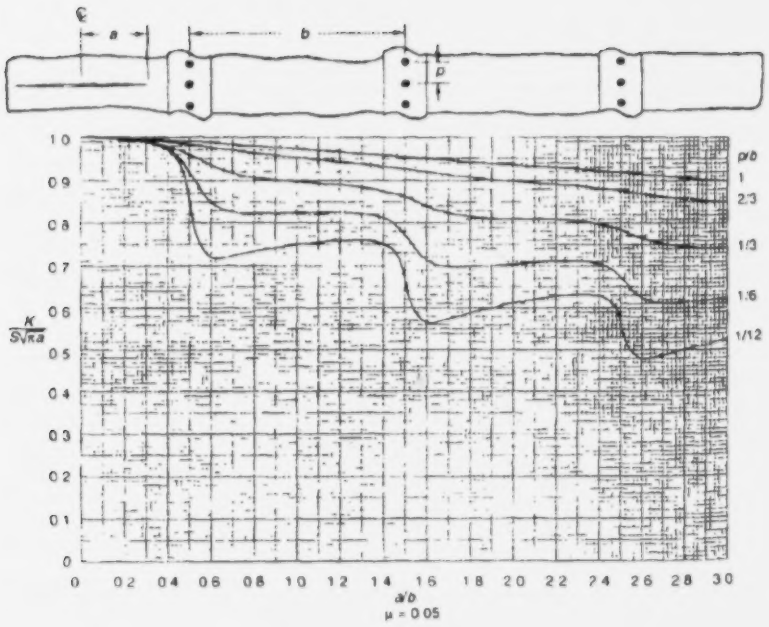

Figure 4-2 Stress intensity modification factors for a one-bay crack centred between two stiffeners [6]

4.2.2 Stiffener Efficiency Factor

The stiffener efficiency factor, γ, is closely related to C' as a description of a stiffener's effectiveness γ is defined as the ratio of the residual strength of a stiffened panel, σ_s, to that of a plain sheet, σ_c

$$\gamma = \frac{\sigma_S}{\sigma_C} \tag{4-4}$$

The value of γ for any type of reinforcement can be determined from its C' factor curve such as shown in Figure 4-2 The stiffener is most effective where the value of C' is at its minimum, C'_{min} That is the C'_{min} is the value for the point at the bottom of the valley in the C' versus a/b curve. The residual strength at this point is thus equal to $\sigma_s = \sigma_c / C'_{min}$, such that $\gamma = 1 / C'_{min}$ Figure 4-3 presents several γ versus μ curves that are reduced from Poe's work It shows again that the effectiveness of a stiffener increases with its relative stiffness parameter

P516758.PDF [Page: 32 of 96]

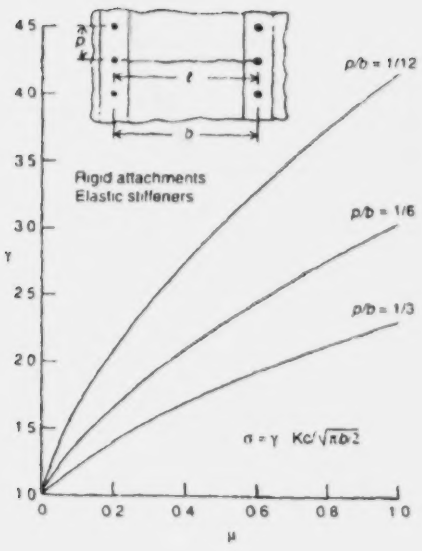

Figure 4-3 Stiffener efficiency factor for a one-bay crack [6]

4 2 3 Load Concentration Factor

Crack tip stress intensity in a stiffened panel is lowered as part of the load is transferred to the stiffener This load is transmitted through the fasteners connecting the panel and the stiffener in case of a riveted or bolted stiffener As the crack grows closer to the stiffener, the stiffener becomes more highly loaded and the shear stress in the fasteners increases The maximum force in a stiffener occurs between the crack and the rivet on either side nearest the crack The force at this location in the stiffener is

$$F = S \cdot L \cdot A \cdot E_s / E \tag{4-5}$$

where F is the maximum force in the stiffener, S is the stress on the panel, L is the stiffener load concentration factor, and A, E_s and E are defined as before L can be defined as the ratio of the maximum local stress to the far-field applied stress on the stiffener A high load concentration can cause yielding or breakage in the stiffener This has detrimental effects on the crack tip stress intensity The most highly loaded fasteners is always the pair that is nearest to the crack tip as most of the load transfer activity actually takes place there Their shear forces Q increase from essentially zero when the

P516758.PDF [Page: 33 of 96]

crack length is zero to a significant value as the crack grows towards the stiffener until the first pair of fasteners yields and subsequently breaks Failure of the other fasteners will then follow This is called fastener unzipping The failure of the stiffener and fasteners has significant effect on the efficiency of the reinforcement They are discussed in more details in Section 4 5

Poe has presented the values of L and Q in his work as shown in Figures 4-4 and 4-5 The stiffener configuration is again for a one-bay crack in the middle of a bay between two stiffeners Note that Q has been normalized In this stiffener configuration, L and Q behave differently under the influence of p, b, and μ Similarly to the C' factor, L decreases as n increases But unlike the C' factor, L increases as p/b decreases The situation in Q is more complicated In this case Q increases as μ increases At low μ, Q increases with decrease in p/b However, the opposite is true at high μ The values of L and Q can be used to plot the residual strength of the stiffener and the fasteners together with the residual strength of the panel This is done in Section 4 5

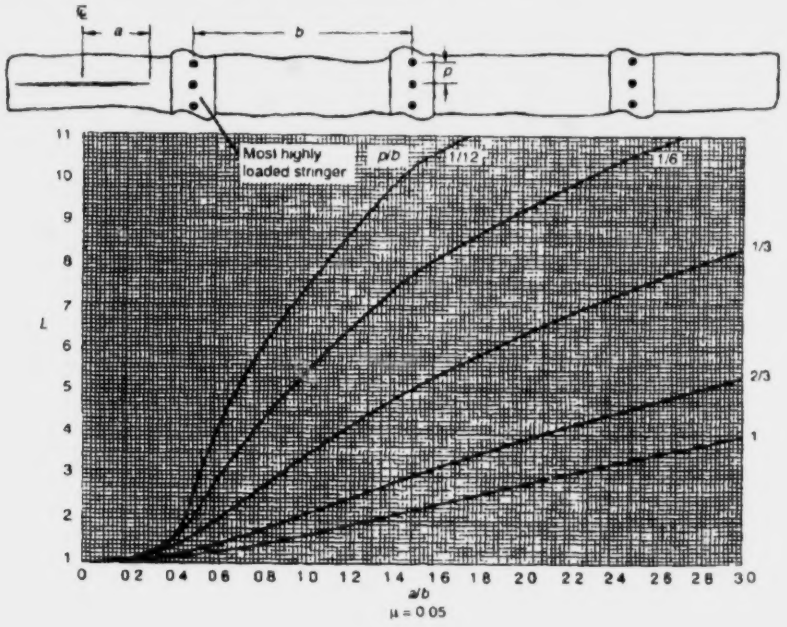

Figure 4-4 Stiffener load concentration factor in most highly loaded stiffener [6]

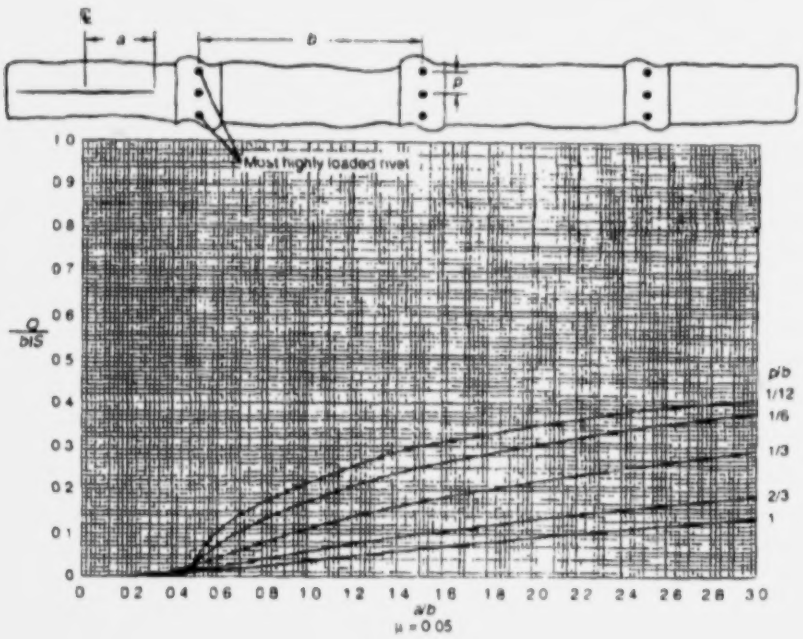

Figure 4-5 Rivet forces in most highly loaded rivets [6]

4.2.4 Method of Estimation

In most design handbooks, only the values of the C factor are provided while for design both L and Q values are necessary. Still, good estimates of L and Q can be obtained from the C factor. The following method is presented in Broek [3]. In an unstiffened plate, the load carried by the plate in front of the crack tip is

$$P = \int \sigma_y t \, dr \tag{4-6}$$

From Equations 2-3 and 2-4, for mode I loading

$$\sigma_y = \frac{K}{\sqrt{2\pi r}} = \frac{Y\sigma\sqrt{\pi a}}{\sqrt{2\pi r}} \tag{4-7}$$

To obtain the load transferred to the stiffener, it is sufficient to integrate Equation 4-6 over a distance of $r = a$

P516758.PDF [Page: 35 of 96]

$$P = \int_{r=0}^{r=a} \frac{tY\sigma\sqrt{\pi a}t}{\sqrt{2\pi r}}\,dr = tY\sigma\sqrt{a/2}\int_{0}^{a} r^{-1/2}\,dr \qquad (4\text{-}8)$$
$$= \sqrt{2}Y\sigma at$$

Thus the additional load carried by the stiffener is P_u (unstiffened) minus P_s (stiffened) and the additional stiffener stress is $(P_u - P_s)/A$. The total stress in the stiffener is $\sigma_t = \sigma + (P_u - P_s)/A$, where σ_t is the total stress and σ is the far-field stress in the stiffener. The stiffener-load-concentration factor $L = \sigma_t/\sigma$ becomes, with Equation 4-8

$$L = 1 + \frac{at\sqrt{2}(Y_u - Y_s)}{A} = 1 + \frac{at\sqrt{2}(1 - C')}{AY_u} \qquad (4\text{-}9)$$

where Y_s and Y_u are the geometric parameters for the stiffened and unstiffened plate. The values of C' and Y_u can be obtained in most design handbooks.

To estimate Q, assume that the entire load is transferred by the closest three fasteners above and below the crack. Together the three fasteners transfer the total load which is $(\sigma_t - \sigma)A$. Typically, the fastener closest to the crack transfer most of the load. Assuming a load distribution of 60%, 30%, and 10% to the three fasteners, then the highest fastener shear load would be

$$Q = 0.6(L - 1)\sigma A \qquad (4\text{-}10)$$

Thus the fasteners must be made strong enough to carry this. It turns out that the actual fastener load on the average is only in the order of 60-70% of the value in Equation 4-10 due to plastic deformation in the fastener hole.

4.3 R Curve of Stiffened Panel

The R curve and crack arrest concepts presented in the last two chapters can be readily combined with the C' factor to illustrate the crack arrest situation in a stiffened structure. Crack arrest occurs in a stiffened structure mainly due to a decreasing strain energy release rate G (or stress intensity factor) that falls below the crack resistance R as the crack approaches a stiffener. Consider a simple case depicted in Figure 4-6 which is a strip bolted to a cracked plate at points A and B. In the presence of the strip, the crack

P516758.PDF [Page: 36 of 96]

surfaces cannot move apart freely as the crack approaches the strip This acts as if the ends of the plate are fixed As mentioned in the last chapter, G decreases with crack length under fixed end condition However this condition is only approximately true in the vicinity of the strip such that if the crack grows past the influence of the strip, G increases again as shown in Figure 4-6 The figure also shows that the largest reduction in G occurs if the crack tip is slightly beyond AB The R curve is shown for plane strain condition for simplicity In the absence of the strip the G curve is straight and the applied stress to produce the G curve shown in the figure would have been high enough to cause fracture However in the presence of the strip, G drops below R and crack arrest occurs when the kinetic energy of the crack is equal to zero

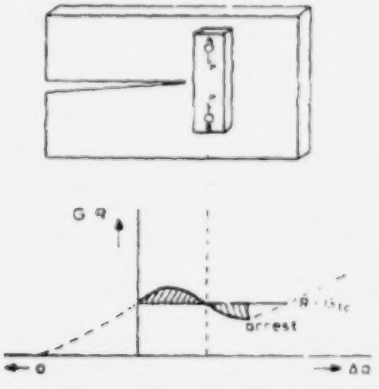

Figure 4-6 Bolted arrest strips [2]

Since G is related to K by Equation 2-5, the C' factor discussed in the last section can be used to construct the G curve of a stiffened structure From Equations 2-5 and 4-4, one obtains $G = C'^2\pi\sigma^2 a/E$ Thus the G curve of a stiffened structure is not a straight line but has a shape as shown in Figure 4-6 since the C' factor varies with crack length. Figure 4-7 depicts a more realistic representation of the energy state of a stiffened panel In this figure the crack has extended to the centre line of the stringer and the R curve is shown to be steeply rising Slow crack growth will commence at a stress σ_i In the absence of the stringer, the G curve at the stress of σ_{cu} would be a straight line as indicated in dashed Thus failure would take place with slow crack growth to B in an unstiffened panel Due to the curve G line however, the stress σ_{cu} will only cause slow

P516758.PDF [Page: 37 of 96]

crack growth to point C The stress must be further raised to σ_{cu} (with simultaneous slow crack growth to D), before final failure takes place At this point G remains larger than R as the crack grows However, if kinetic energy is taken into consideration, fracture could occur at a lower stress

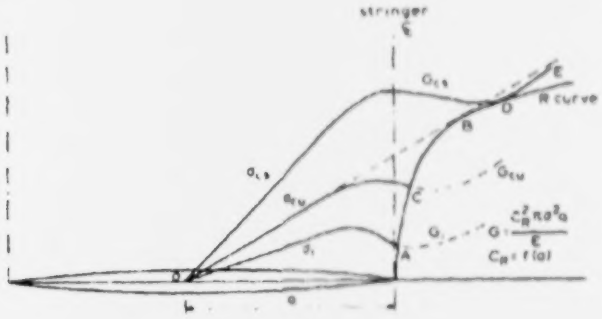

Figure 4-7 *R* curve concept for stiffened panel (crack extending to stringer) [2]

For the case of a short crack in a stiffened panel, the situation is more complicated as depicted in Figure 4-8 As the crack is far away from the stringer, the G curve is straight until it reaches the vicinity of the stringer Slow Stable crack growth starts at a stress σ_i and is arrested almost immediately at A Since the part OA of the curve G_i is still straight, slow growth commences at the same stress σ_i as in the unstiffened panel At the stress σ_{cu} unstable crack growth occurs, since the line G_{cu} is tangent to the R curve at point B Since the part OB of the curve is also straight, σ_{cu} is the fracture stress in the unstiffened panel However, fracture does not occur in the stiffened panel as unstable crack growth is arrested at C as the G curve drops below the R curve under the influence of the stringer More slow crack growth follows as the stress increases until fracture occurs at stress σ_{cs}, where G remains larger than R after point E Again, any contribution of kinetic energy, and any rate effect on R is disregarded, which could result in a lower fracture stress in the stiffened panel than depicted In reality the R curve for a stiffened and unstiffened panel need not, and should not, be the same Also stringer failure and fastener failure have not been incorporated into the foregoing figures These issues are addressed in Section 4 5

P516758.PDF [Page: 38 of 96]

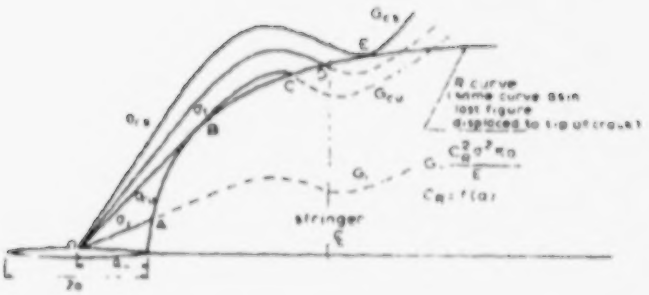

Figure 4-8 *R* curve concept for stiffened panel (short crack) [2, modified]

4.4 *Residual Strength of Stiffened Panel*

The residual strength diagram provides a convenient means of determining the fracture stress of a stiffened structure The calculation of the residual strength of a cracked stiffened panel is based on the residual strength properties of an unstiffened case by incorporating the C' factor From Equation 4-4, one obtains the residual strength of a stiffened structure as $\sigma_c = K_c / C' Y \sqrt{\pi a}$ The residual strength of stiffened and unstiffened panel is plotted against crack length in Figure 4-9 The residual strength of the stiffened panel has the same basic shape as the C' factor curve When the crack is small and remote from the stringer, the influence of the stringer is small and the residual strength of the stiffened case is the same as that of the unstiffened case However, as the crack grows in length, there is a continuous decrease in residual strength of the unstiffened panel while the residual strength increases as the crack approaches the stringer The difference in residual strength between the two cases is the greatest at a point slightly beyond the centre line of the stringer After that point the residual strength of stiffened panel starts to decrease. Consider a crack of size a_2 in the stiffened panel If a stress of σ_2 is applied to the panel, unstable crack growth will commence, as the residual strength is lower than σ_2 as the crack grows in length However when the crack grows to a length of a_1, the residual strength is again equal to σ_2 and it increases afterwards In order for fracture to continue, the applied stress must be increased Thus, under constant applied stress of σ_2, the crack is arrested by the stringer at a crack length of a_1 Based on the same reasoning, it can be seen that the stringer is able to arrest any

P516758.PDF [Page: 39 of 96]

crack with a length between a_c and $\bar{a}$, where the residual strength is less that $\bar{\sigma}$, the maximum value of residual strength that can be provided by the stringer. For a crack size less than a_c (a_1 for example), the residual strength, or fracture stress, is higher than $\bar{\sigma}$ such that crack arrest is not possible if the fracture stress is reached and maintained. It can be concluded from the residual diagram that stiffened structures can sustain larger damage. Whereas, at an applied stress of $\bar{\sigma}$, the unstiffened panel would fail with a crack size of approximately a_c, the stiffened panel can tolerate a larger crack size up to $\bar{a}$.

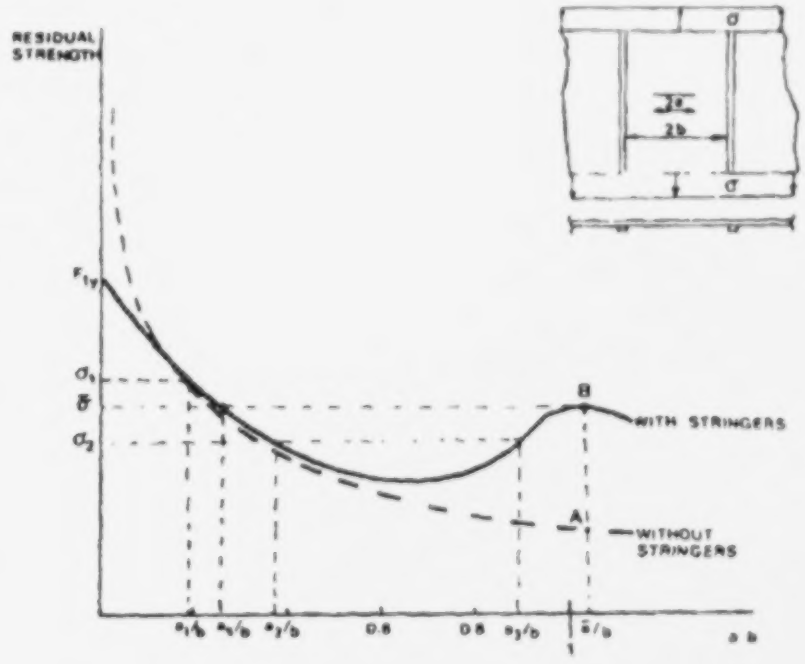

Figure 4-9 Residual strength diagram of stiffened panel [3, modified]

The foregoing discussion has ignored the residual strength of the stiffener and the fasteners. However, if the stress concentration in the stiffener and fasteners is sufficiently high to cause yielding and failure, then their residual strengths have to be taken into consideration. The detrimental effects of stiffener and fasteners failure have on the fracture characteristics of the stiffened panel are discussed in more details in Section 4.5. For now the residual strength of the stringer shown in Figure 4-9 is plotted together with residual strength of the stiffened panel in Figure 4-10(a). The residual

strength of the stringer, σ_{ys}, can be determined by its load concentration factor, l_s, and its tensile strength, σ_t, that is $\sigma_{ys} = \sigma_t l_s$. The residual strength of the fastener can be calculated similarly using its own load concentration factor. In Figure 4-10(a), a crack of size a_1 can be arrested at a_2. At this point, further increase in stress leads to stringer fracture at crack size $\bar{a}$ and stress $\bar{\sigma}$. The stringer becomes ineffective and total fracture of the panel occurs. Thus, due to stringer fracture, the crack arrest stress is lower than the maximum possible value, which at the peak of the residual strength curve of the panel. This is an undesirable situation, as part of the stringer's crack arrest ability is not realized. One way to improve this situation is to select a stringer material with a higher tensile strength as shown in Figure 4-10(b). In this case fracture of the panel occurs before the stringer fails.

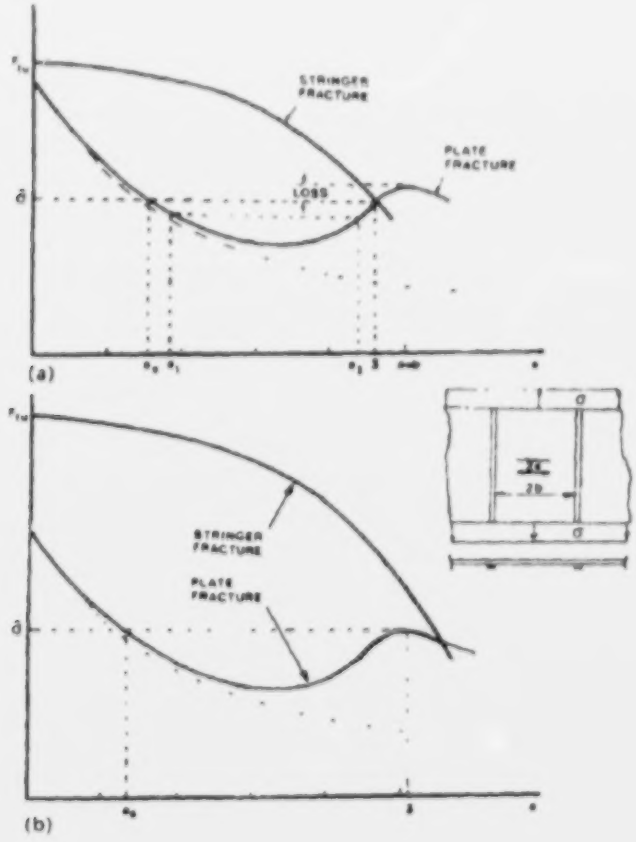

Figure 4-10 Effect of stringer on residual strength diagram (a) Stringer critical; (b) Plate critical [3, modified]

P516758.PDF [Page: 41 of 96]

4.5 Crack Arrest Parameters

In Section 4 2, several factors have been identified as having significant effects on the stiffener's efficiency They are the attachment spacing, reinforcement spacing, and the relative stiffness parameter Similarly, the failure of the stiffener and the fasteners affect the overall effectiveness of a stiffened structure and are discussed in this section In addition, the dynamic aspect of fracture in stiffened structure, which has been largely ignored up to this point, is addressed in this section The fracture behaviour of integral and welded stiffeners, which differs from that of riveted and bolted stiffeners, is also presented in this section

4 5 1 Dynamic Effects

Throughout this chapter the contribution of kinetic energy as a crack driving force has been ignored This can be justified by test data on stiffened panels showing that the contribution of kinetic energy as a crack driver is small There are two reasons for this The most important is that when the crack passes the intact stringer a large amount of plastic deformation energy is absorbed by the stringer, so that the apparent energy required for crack advance is much larger than the skin crack resistance R This is shown in Figure 4-11 This deformation energy is far greater than the kinetic energy even for large amounts of crack growth A second reason is that the R curve for a stiffened panel is steeply rising As the kinetic energy is represented by the area between the G curve and the R curve the kinetic energy tends to be small This also implies that the growth rate of the unstable crack is relatively slow in a stiffened panel

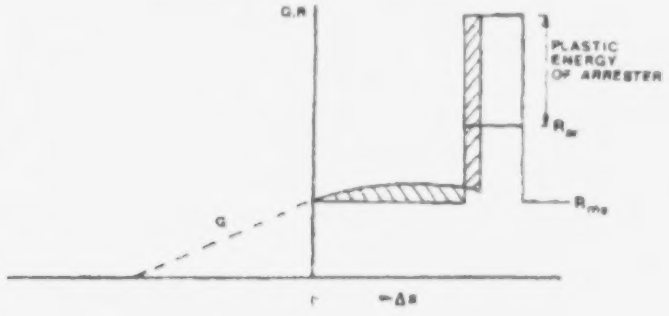

Figure 4-11 Stiffener plastic deformation [3]

4.5.2 Integral and Welded Stiffeners

Although this chapter is mainly focused on mechanically fastened stiffeners, the materials presented are also suitable for integral and welded stiffeners by considering very close fastener spacing. However, there are two fundamental differences in crack arrest behaviour between integral and welded stiffeners and mechanically fastened stiffeners. First, in case of a fatigue crack, crack arrest in mechanically fastened stiffeners can be achieved when the crack runs into a fastener hole. In case of integral or welded stiffeners, this option is not possible. In fact, there is no real crack arrest, but only a reduction of crack growth rate. Despite having no arrest in fatigue cracking, the overall crack propagation is slower in integral or welded stiffener. Second, in mechanically fastened stiffener, the skin crack grows under the stiffener so that the stiffener can remain intact. For integral or welded stiffener, the crack advances by growing into the stiffener and thereby severing it. The stiffener then loses its efficiency. In general, the crack arrest capabilities for integral or welded stiffeners are not well understood and test data of this type are limited.

4.5.3 Stiffener Yielding

The efficiency of a stiffener drops once it starts to yield. This is particularly evident for stiffener having a small cross-sectional area. Figure 4-12 is a plot of the stiffener efficiency for various relative stiffnesses μ against the applied stress for a one bay crack. In the figure F_{ys} is the yield stress of the stiffener. For a stiffener having a large μ, it can be seen that until the stiffener begins to yield, the yield stress does not play a role. The efficiency is constant up to an applied stress that is close to the stiffener's yield stress. After that point, there is a rapid drop in efficiency down to 1.0 at the stiffener's yield stress. However, for a stiffener having a small cross-section area (small μ), the drop in efficiency starts much earlier at a lower ration of applied stress to yield stress. Thus, when the effects of yielding are included, the difference in stiffener efficiency between the different sizes is very significant.

P516758.PDF [Page: 43 of 96]

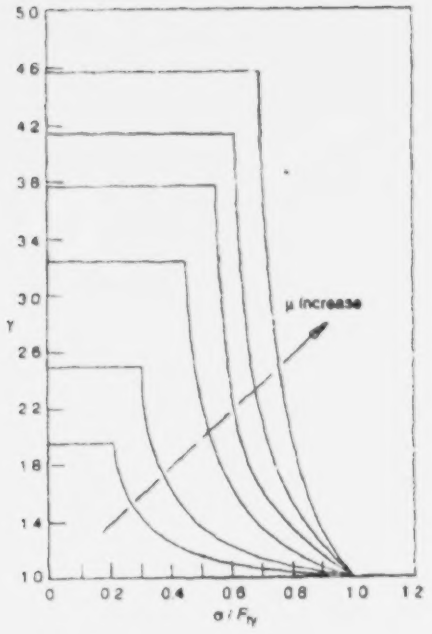

Figure 4-12 Effects of applied stress levels on the stiffener efficiency [6]

4.5.4 Broken Stiffener

Due to high stress concentration at the crack tip, the stiffener may break if its tensile strength is exceeded. In that case, not only is the stiffener no longer effective, the loads carried by the stiffener is also fed back into the cracked sheet, causing the stress intensity at the crack tip to increase instead of decrease. Consider the case of a two-bay crack with a centre broken stiffener shown in Figure 4-13. The stiffener efficiency factor of the intact edge stiffener γ is plotted against the relative stiffness parameter μ. γ is obtained by superposition of two separate cases, the case without a centre stiffener and the case involved with a broken stiffener alone. The stress intensity modification factor for the broken stiffener, C'_b, is shown in Figure 4-14. Figure 4-13 shows that γ increases with μ up to a point. Since the load carried by the stiffener increases with μ, the feed back load by the broken stiffener into the sheet increases also. At some point the stress intensity increase by the feed back load becomes greater than the reduction provided by the intact stiffeners, and their efficiencies decrease. Figure 4-13 also shows that a small

P516758 PDF [Page: 44 of 96]

stiffener can be just as effective as a large stiffener in case of having a broken central stiffener This could mean a saving of materials in stiffener design

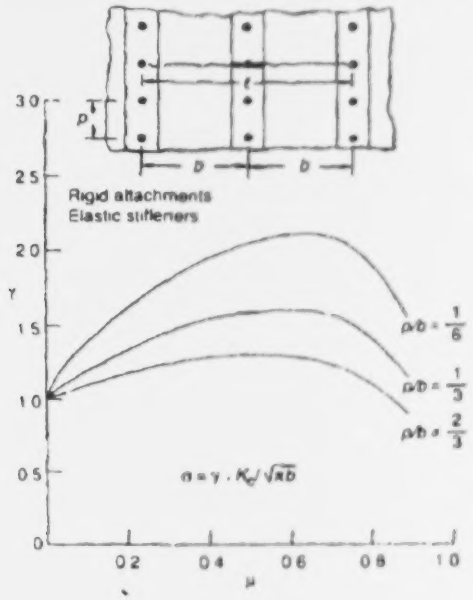

Figure 4-13 Stiffener efficiency factor for a two-bay crack with a centre broken stiffener [6]

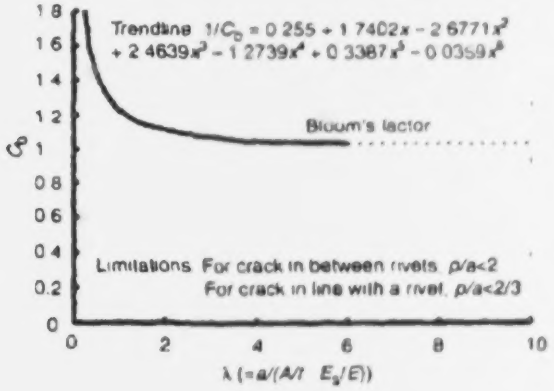
Trendline $1/C_b = 0.255 + 1.7402x - 2.6771x^2 + 2.4639x^3 - 1.2739x^4 + 0.3387x^5 - 0.0359x^6$
Bloom's factor
Limitations For crack in between rivets $\rho/a<2$
For crack in line with a rivet, $\rho/a<2/3$
$\lambda (=a/(A/t \ E_s/E))$

Figure 4-14 Effect of broken stiffener on stress intensity factor [6]

Now consider the residual strength diagram of the same situation shown in Figure 4-15 In this figure the failure curves of the skin, edge stiffener, and central stiffener are shown as curves f, g, and k respectively, if the central stiffener remains intact The maximum crack arrest capability of the panel is then at L with a crack arrest stress of $\overline{\sigma}$

P516758.PDF [Page: 45 of 96]

If the central stiffener is broken, then the skin and the edge stiffeners must carry extra load from the failed stiffener. Thus their failure curves f and g are lowered to f' and g', shown as dashed lines in Figure 4-15. The crack arrest stress is then reduced to the intersection of f' and g' at H'.

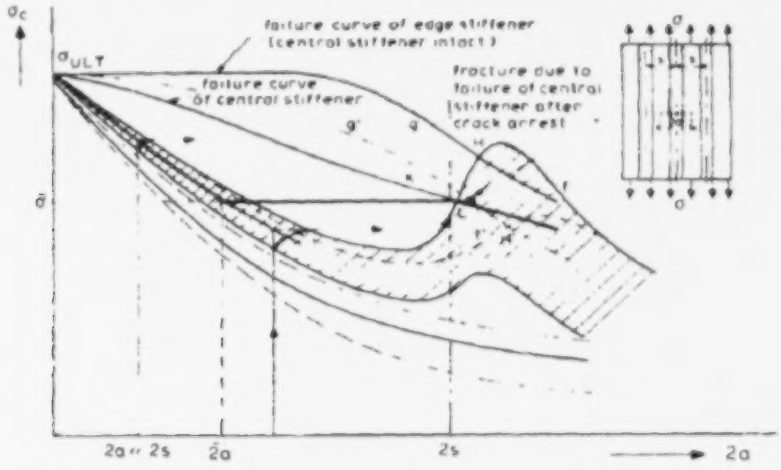
failure curve of edge stiffener (central stiffener intact)
failure curve of central stiffener
fracture due to failure of central stiffener after crack arrest
2a = 2s
2a
2s
2a

Figure 4-15 Residual strength diagram for a panel with three stringers and a central crack [2]

4.5.5 Fastener Failure

Similar to the stiffener, the fasteners that transfer the load from the skin to the stiffener experience increasing stress as the crack tip approaches. If the fastener loads become too high, fastener failure may take place by shear. When this occurs, the fastener is no longer effective in transmitting loads, causing the stress to increase in the skin and decrease in the stiffener. The residual diagram for this situation is depicted in the Figure 4-16. In this figure the residual strength of the fastener is included, which can be calculated from its shear strength and its load concentration factor. In the course of crack arrest, the shear strength of the fastener is exceeded at the intersection of curve f and h. Fastener failure causes the stress to rise in the skin and reduce in the stringer and their corresponding failure curve is lowered to f' and raised to g' respectively. The point of crack arrest is then lowered from H to H'.

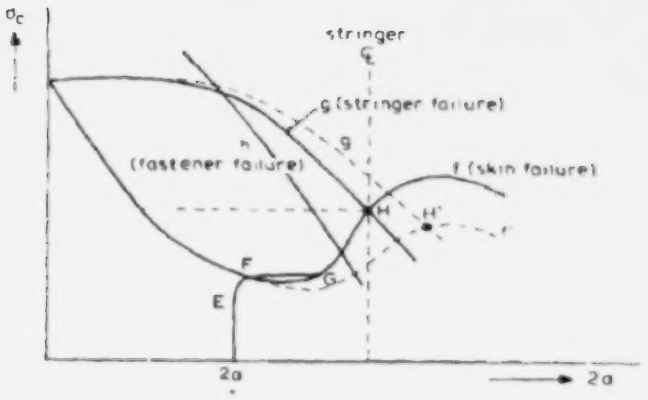

Figure 4-16 Criterion for fastener failure [2]

P516758.PDF [Page: 47 of 96]

5 Methods of Analysis

5.1 Introduction

In a stiffened panel, the crack tip stress intensity is reduced because a portion of the skin load is transmitted through the fastener and to the stiffener Therefore the general stress intensity factor for a stiffened panel can be written as the stress intensity factor of caused by the applied stress in an unstiffened case minus the stress intensity contribution from the fastener forces For an infinitely wide panel, the K expression can be written as

$$K = \left[\sigma - \sum_{i=1}^{n} f(F_i) \right] \sqrt{\pi a} \tag{5-1}$$

where F_i is the fastener load of the ith fastener and all other variables are defined as before Thus, the main objective of any study on stiffened structure is to determine these unknown fastener forces These can be solved by either analytical or numerical methods An analytical method has the advantage of allowing direct solution of the problem for any crack size The effect of different panel parameters on the residual strength of a certain panel configuration can be more easily assessed, so that the stiffened panel can be optimized In the case of a numerical method, a new analysis has to be carried out when the configuration is changed because a new set of approximation equations has to be generated for each configuration However, it is possible to obtain a closed-form analytical solution for only a limited number of simple configurations In most instances, the problem has to be solved numerically A numerical method also has the advantage of possibly incorporating stringer eccentricity and hole deformation In this chapter, three numerical analysis methods are presented· finite element method, boundary element method, and finite difference method In general, both analytical and numerical methods give almost identical results

5.2 Analytical Methods

The general procedure for any analytical investigation of stiffened structures is first presented An approximate method that provides a quick estimation of the residual

P516758.PDF [Page: 48 of 96]

strength follows Several investigators use more advanced analytical equations to solve different stiffener configurations and examine stiffener parameters They are presented at the end of this section

5 2 1 Vlieger and Poe's Method

Vlieger and Poe [2] developed a procedure for the analytical calculation by splitting up the stiffened panel into its components, the skin and the stringer The fasteners are replaced by their corresponding reaction forces acting on the skin and the stiffener, F_1 F_n They are depicted in the upper line of Figure 5-1, where the fastener forces are shown to oppose the applied stress on the skin and thus reducing the stress intensity The fastener forces act in the same direction as the applied stress on the stiffener and leads to stress concentration in the stiffener The problem is then reduced to that of an unstiffened plate loaded by a uniaxial stress σ and fastener forces F_1 F_n This case can in turn be considered as a superposition of three others as shown in the second line of Figure 5-1

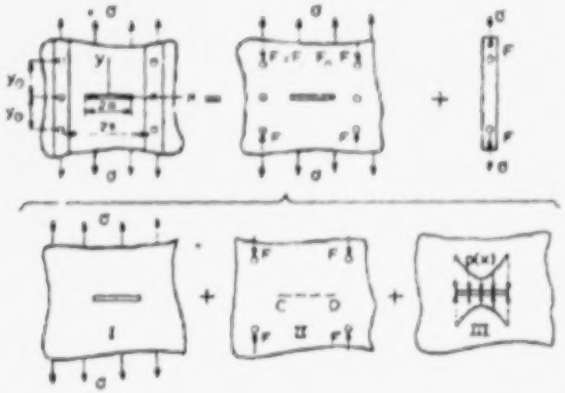

Figure 5-1 Analytical solution for stiffened sheet [2]

In the figure, Case I is a cracked sheet loaded with the applied stress only Case II is a sheet without a crack, loaded with the fastener forces F_1 F_n Case III is a crack sheet loaded with forces on the crack edges given by the distributed load $p(x)$ $p(x)$ represent the forces between points C and D in case II that have to be exerted to provide the necessary stress-free crack edges when the slit CD is cut The expression for $p(x)$ is

P516758.PDF [Page: 49 of 96]

given by Love [2] The stress conditions at the crack tip in these three cases have to be determined and the crack tip stress intensity factors are given in Equations 5-2

$$\begin{aligned}
&\text{I} \quad K_\sigma = \sigma\sqrt{\pi a} \\
&\text{II} \quad K = 0 \\
&\text{III} \quad K_P = \frac{-2\sqrt{\pi a}}{\sqrt{\pi}} \int_0^a \frac{p(x)dx}{\sqrt{a^2 - x^2}} \\
&\text{where} \quad p(x) = \frac{F_{y_0}}{\pi B\left[y_0^2 + (x-s)^2\right]}\left[\frac{3+\nu}{2} - (1+\nu)\frac{(x-s)^2}{y_0^2 + (x-s)^2}\right] + \\
&\qquad\qquad \frac{F_{y_0}}{\pi B\left[y_0^2 + (x-s)^2\right]}\left[\frac{3+\nu}{2} - (1+\nu)\frac{(x+s)^2}{y_0^2 + (x+s)^2}\right]
\end{aligned} \tag{5-2}$$

B = thickness of skin

The fastener forces are solved by the displacement compatibility requirement between the sheet and stiffener at the corresponding fastener locations By equating the displacement of the sheet and stiffener at these location, a set of n (n = number of fasteners) independent algebraic equations is obtained, from which the fastener forces can be solved When the fastener forces F are known, the stress intensity modification factor C' and the stiffener load concentration factor L can be calculated as follows (A is the cross sectional area of the stiffener)

$$C' = \frac{K_\sigma + K_F}{K_\sigma} \tag{5-3}$$

$$L = 1 + \frac{F}{\sigma A} \tag{5-4}$$

5 2 2 Crichlow's Method

Another analytical method using the finite width concept has been proposed by Crichlow [2] It is a very simple approximate method for the unstiffened panel based on the idealized stress distribution shown in Figure 5-2, where σ_{nom} is the far-field applied stress on the panel The crack tip stress concentration is approximated by an average stress σ_{tip} over a distance of w_e in front of the crack tip w_e is called the effective width,

and is supposed to be a material constant that has to be determined from experiments By equating σ_{nom} across the width of the panel to the stress across the crack plane, one obtains

$$(\sigma_{tip} - \sigma_{nom})2w_c = 2a\sigma_{nom} \tag{5-5}$$

Fracture is assumed to occur when σ_{tip} is equal to the ultimate tensile strength of the material, σ_u At this point the crack size is assumed to have a critical length of a_c The fracture stress σ_c is thus given by

$$(\sigma_u - \sigma_c)w_c = \sigma_c a_c \tag{5-6}$$

or

$$\sigma_c = \sigma_u \frac{1}{1 + a_c / w_c} \tag{5-7}$$

Figure 5-2 Effective width concept [2]

In the case where the crack tip is close to a stiffener, Equation 5-6 is modified to give the fracture stress σ_{cs} as

$$(\sigma_u - \sigma_{cs})(w_c B + \rho A) = \sigma_{cs} a_c B \tag{5-8}$$

where A is the stiffener cross sectional area, ρ is a factor accounting for stiffener eccentricity, and B is the skin thickness The fracture stress is

$$\sigma_{cs} = \sigma_u \frac{1}{1 + \dfrac{a_c}{w_c + \rho A / B}} \tag{5-9}$$

P516758.PDF [Page: 51 of 96]

Crichlow's method provides a quick estimate of the residual strength of a stiffened panel If the fracture toughness K_c for the unstiffened skin is known, then w_c for a crack equal to the stiffener spacing ($2a = s$) can be calculated from

$$\sigma_c = \frac{K_c}{\sqrt{\pi s/2}} \tag{5-10}$$

Combining Equations 5-7 and 5-10 with $a_c = s/2$ gives

$$w_c = \frac{s/2}{\frac{\sigma_u \sqrt{\pi s/2}}{K_c} - 1} \tag{5-11}$$

The residual strength of the stiffened panel can then be calculated with Equation 5-9 using w_c determined in Equation 5-11 It should be emphasized that this is only an approximation and a more sophisticated analysis such as one presented in the previous section will be required to obtain a better impression of the residual strength behavior and of the possibilities for crack arrest

5 2 3 Mixed Mode Loading Analysis

Sethuraman and Maiti [12] performed a parametric study on a crack-stiffened panel with bonded stiffeners The parameters involved the stiffener location, stiffener length, shear modulus of the stiffener, shear modulus of adhesive and thickness of adhesive The basic unknown in the problem is the shear stresses which develop at the interface between the sheet and the adhesive (or between the adhesive and the stiffener) They can be determined by the compatibility between the displacement of the sheet and the deformation of the stiffener Both mode I and mode II loading were studied in their investigation

P516758.PDF [Page: 52 of 96]

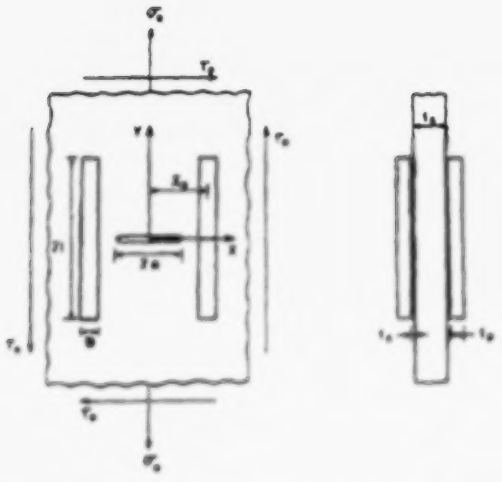

Figure 5-3 Symmetrically crack-stiffened rectangular panel under mixed mode loading [12]

The configuration considered in a symmetrically crack-stiffened rectangular panel with the stiffeners bonded on both sides of the panel as shown in Figure 5-3 For both types of loading the problem was divided as shown in Figures 5-4 and 5-5 into the cracked sheet with loading (b), the stiffener with loading (c) and the adhesive with loading (d) In all the cases, the shear stress in the adhesive was assumed to be constant along its thickness and along the width of the stiffener

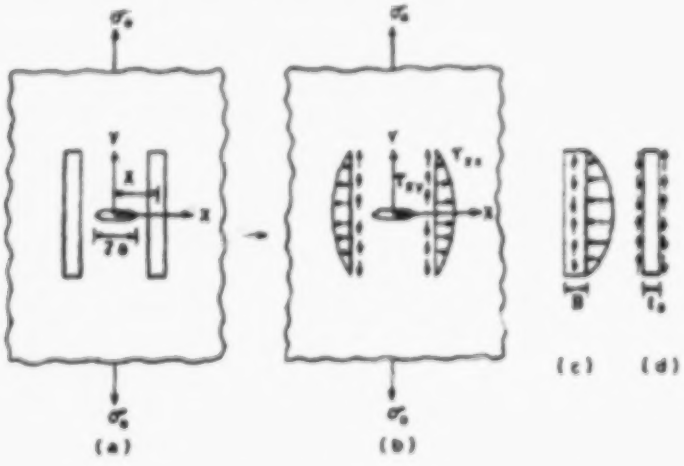

Figure 5-4 Mode I part of loading and its break-up [12]

P516758.PDF [Page: 53 of 96]

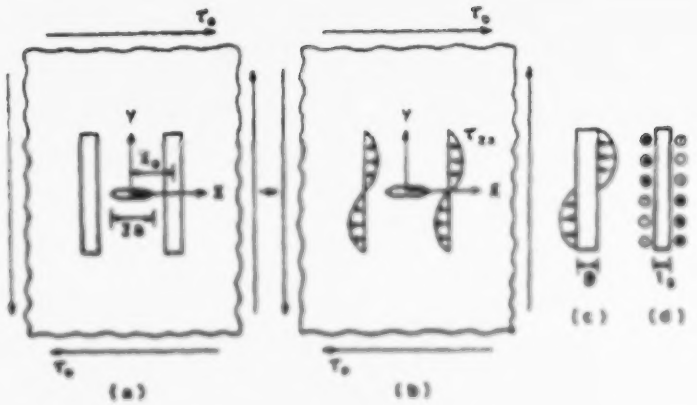

Figure 5-5 Mode II part of loading and its break-up [12]

The adhesive thickness is much less than the thickness of the plate or stiffener and the adhesive shear stress, τ_{A} and τ_{A} in Figures 5-4 and 5-5, can be related to stiffener and sheet centre displacements These relations were treated as compatibility conditions The sheet displacement due to the external loading was obtained using Westergaard complex stress function and the displacement due to the stiffener forces was obtained using the Green's function approach This is similar to the second line of Figure 5-1 The longitudinal displacement of the stiffener due to longitudinal shear stress was obtained using the equilibrium and stress-strain-displacement relationship The transverse displacement was obtained from elementary beam theory The displacements were obtained for both mode I and mode II loading The unknown shear stresses were then determined by substituting the displacement into the compatibility conditions For mode I loading

$$\zeta\tau_{A} = u_{pl} - 2B\int_0^{l}\left(S_1\tau_{A} + S_2\tau_{A}\right)dy_0 - R_1 \tag{5-12}$$

$$\zeta\tau_{A} = \frac{1}{E_p t_p}\int_0^{y}\int_y^{l}\tau_{A}(dy)^2 - 2B\int_0^{l}\left(S_3\tau_{A} + S_4\tau_{A}\right)dy_0 - R_2 \tag{5-13}$$

where

$$\zeta = \frac{t_a}{Gi_a} + \frac{t_s}{4Gi_s} + \frac{3t_p}{8Gi_p}$$

P516758.PDF [Page: 54 of 96]

In Equations 5-12 and 5-13, the subscripts a, p, and s stand for adhesive, stiffener, and sheet respectively. u_{p1} is the mode I displacement of the stiffener. y_0 is a point where a concentrated force acts in the Green's function. E and G are the Young's and shear modulus respectively. N_i's and R_i's are displacement functions due to a set of four point loads and the external tensile load respectively. t, B and l are defined in Figure 5-3. Sethuraman and Maiti assumed τ_{xy} and τ_{yz} to be polynomial of N degree. Equations 5-12 and 5-13 then give a set of $2N$ simultaneous equations to solve for the unknown coefficients in τ_{xy} and τ_{yz}. After the determination of the shear stresses, the stress intensity factor is calculated using the superposition principle of the external loads and the shear stresses in an equation resembling Equation 5-1.

Using Equations 5-12 and 5-13, Sethuraman and Maiti [12] performed a parametric study of the panel shown in Figure 5-3 with a crack length of $2a$ = 25 mm. A plot of stress intensity factor K for mode I problem against the stiffener location is shown in Figure 5-6. It indicates there is a location of maximum K reduction. The same trend can be observed for the mode II problem and this location is close to the crack-tip and on the side opposite the ligament. The influence of the stiffener length and shear modulus and the effects of the adhesive thickness and shear modulus on K were similarly evaluated. The result showed that increasing the stiffener length is advantageous up to a certain limit, but it does not give any further benefit when l/a is more than 1.20. Increasing the shear modulus of the stiffener decreases K. This is analogous to increasing the relative stiffness parameter μ mentioned in the last chapter. The reduction in thickness and increase in shear modulus of the adhesive causes more load transfer from sheet to the stiffener and leads to more reduction in K.

P516758.PDF [Page: 55 of 96]

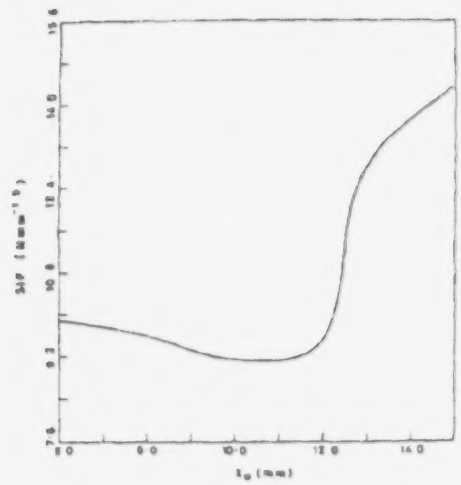

Figure 5-6 Variation of stress intensity factor with stiffener location for mode I problem [12]

5.2.4 Multiple Cracks Analysis

Nishimura [8] analyzed a model of a multiple cracked sheet attached with riveted stiffener subjected to remote uniaxial stress as shown in Figure 5-7. The stiffeners in three different conditions were considered: intact, broken, and cracked. The problem is solved by using Fredholm integral equations which are derived from the solution of a single crack and unknown density of surface traction along each crack. The surface tractions and fastener forces are determined from a system of equations generated by the Fredholm integral equations on equilibrium of crack traction and compatibility equations of displacements among the sheet, fasteners and stiffeners. The stress intensity factor can then be calculated from these forces.

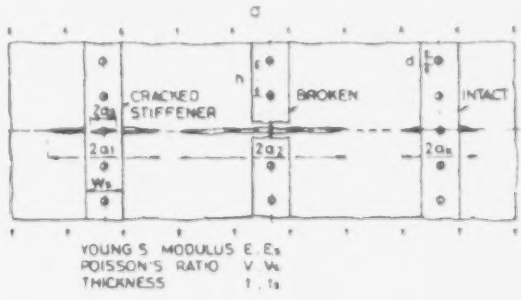

Figure 5-7 Model of a multiple cracked sheet attached with riveted stiffeners [8]

P516758.PDF [Page 56 of 96]

The displacements in the cracked sheet were again determined by superposition of three cases as shown in Figures 5-8(*a*), (*b*), and (*c*). V_1 is the displacement of an uncracked sheet subjected to remote uniaxial stress and it is given by

$$V_1(x,y) = \sigma y / E \tag{5-14}$$

where E is the Young's modulus of the sheet. V_2 is the displacement due to a pair of fastener loads. V_3 is the displacement obtained by applying an equal and opposite stress distribution over the crack face to cancel out the stress distribution ($\sigma - \sigma_y$) caused by remote tensile stress and fastener forces F. V_3 is expressed in terms of the unknown densities of surface traction P_k using the Westergaard complex stress function in the cracked sheet due to a pair of concentrated forces applied to the crack faces. The total sheet displacement was then given by the sum of the three cases

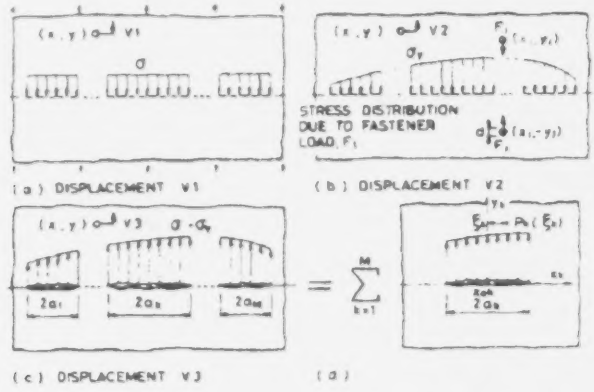

Figure 5-8 Three cases for skin displacement [8]

The nth fastener displacement due to the fastener reaction force F_i is given by

$$V_{Ri} = F_i \cdot f \tag{5-15}$$

where f denotes the fastener flexibilities. The displacements for the intact, broken, and cracked stiffeners were determined by summing the displacements due to fastener forces V_{Fi} and remote stress V_1. For the intact stiffener subjected to gross stress σ_s(= $\sigma E_s / E$) and direct fastener forces F, V_{Fn} and V_{1n} are given by

P516758.PDF [Page: 57 of 96]

$$V_{Gi} = \sigma_s y_i / E_s \tag{5-16}$$

$$V_{Di} = 1/(W_s t_s E_s) \cdot \left(\sum_{j=1}^{i} F_j y_j + y_i \sum_{j=i+1}^{N} F_j \right) \tag{5-17}$$

where W_s, t_s and E_s are the width, thickness, and Young's modulus of the stiffener, and N is the number of active fasteners per stiffener. Equation 5-17 is analogous to the familiar mechanics equation for axial displacement, $\Delta = PL/AE$. The displacements of the broken and cracked stiffener were similarly determined. The stress intensity factor for the cracked stiffener was also expressed in terms of the gross stress and fastener forces.

From the equilibrium (stress free) condition on each crack surface, Fredholm integral equations are derived in terms of the unknown tractions of the crack surfaces and fastener forces as follows

$$\begin{aligned} & P_i(\xi_i) - \sum_{k=1}^{M}{}^{*} \int_{-a_k}^{a_k} P_k(\xi_k) g(x_i - x_{0k}, \xi_k) \, d\xi_k \\ & = \sigma - \sum_{j=1}^{N} F_j (1+\nu) y_j \alpha(x_j, y_j, x_i)/(2\pi) \\ & |\xi_i| < a_i, \quad i = 1,2,\ldots M \end{aligned} \tag{5-18}$$

where g and α are functions in the stress equation and the symbol $\sum^{*}$ means the terms corresponding to $k = i$ has been excluded in the summation. The compatibility equations are derived from the compatibility of displacements at the junction line of the fastener arrays. The corresponding equations for intact, cracked and broken stiffeners are as follows

$$\left\{ V_1 + \sum_{j=1}^{N} V_2 + V_3 \right\}_i = \{ V_R + V_{Gi} + V_D \}_i \tag{5-19a}$$

$i = 1,2,\ldots N$

for intact/cracked stiffeners, and

$$\left\{ V_1 + \sum_{j=1}^{N} V_2 + V_3 \right\}_i - \left\{ V_1 + \sum_{j=1}^{N} V_2 + V_3 \right\}_N = \{ V_R + V_{Gi} + V_D \}_i \tag{5-19b}$$

$i = 1,2,\ldots N$

P516758.PDF [Page: 58 of 96]

for broken stiffeners Equations 5-18 and 5-19 form a system of simultaneous equations from which the unknown surface tractions P and fastener forces F are determined The crack tip stress intensity factors of the sheet and the cracked stiffener were then calculated from P and F

To demonstrate the applicability of the proposed method, Nishimura [8] performed two numerical examples as shown in Figure 5-9 In both cases, the stress intensity factors (SIF) for a panel containing a single crack and multiple cracks are compared For case (a), the SIF of the sheet was calculated for all three stiffener conditions as shown in Figure 5-10(a) The plot of the SIF of the sheet against crack length is shown in Figure 5-10(b) In both cases the SIF of multiple cracks in the stiffened sheet was found to be larger than that of a single crack As shown in Figure 5-10a, the SIF of the sheet increases as the stiffener becomes more damaged Nishimura also defined a mutual interaction factor F_M as a stress intensity ratio of the multiple cracks to the single crack As shown in Figure 5-11, this factor is smaller in a stiffened sheet than an unstiffened sheet due to the load transfer to the stiffener

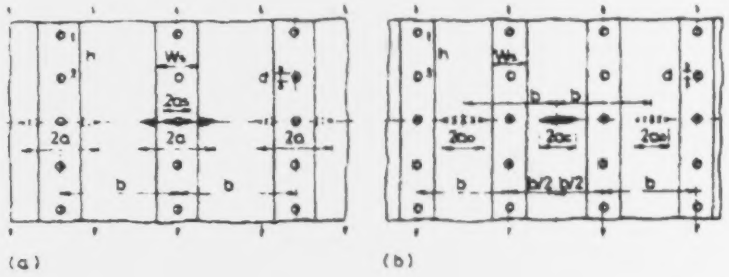

Figure 5-9 Two numerical examples [8]

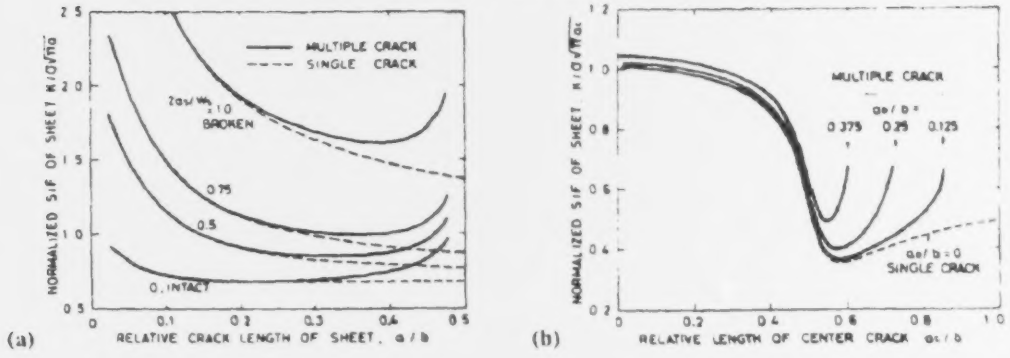

Figure 5-10 Variation of stress intensity factor with relative crack length [8]

P516758 PDF [Page: 59 of 96]

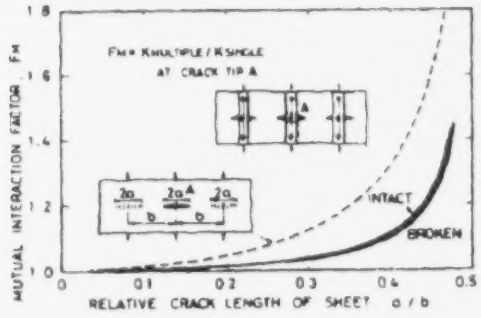

Figure 5-11 Variation of mutual interaction factor with crack length [8]

5.3 *Finite Element Method*

In the finite element method, the structure of interest is discretized into simple geometric shapes called finite elements. The elements are connected at node points where continuity of the displacement fields is enforced. Within the element, the material properties and the displacements are interpolated using polynomials called shape functions and are expressed in terms of unknown values at the element nodes. From the strain-displacement compatibility relationship and the stress-strain constitutive law, the stiffness matrix is obtained for each element. The elemental stiffness matrices are assembled to give the global stiffness matrix. By considering the global loading and displacement constraints, a set of equations is generated. Solution of these equations gives the approximate behavior of the structure.

5.3.1 Shear Element

Shear element is a special membrane type element commonly used to represent both the sheet and the stiffener and the adhesive in the finite element analysis of stiffened panel. One such element is a triangular element with constant shear strain field developed by Sethuraman and Maiti [13] to model the adhesive behavior in a doubly bonded stiffened panel. It incorporates the shear deformations of the sheet and the patch as well as the adhesive.

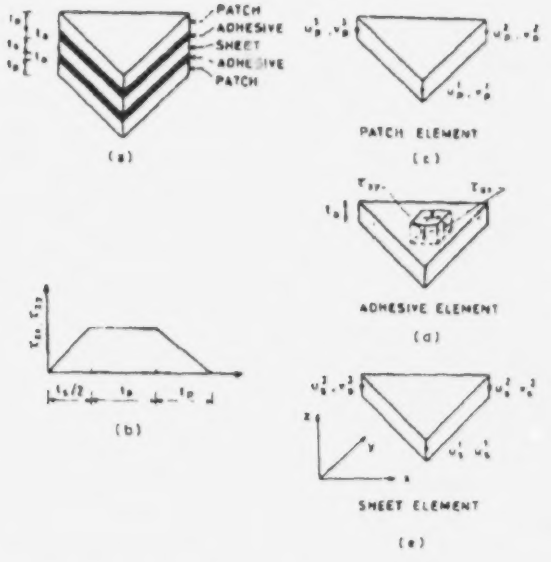

Figure 5-12 (a) Stiffener-adhesive-sheet composite element; (b) variation of shear stresses along the thickness direction; (c), (d) and (e) break-up of the composite element shown in (a) [13]

The element geometry is shown in Figure 5-12 It has six nodes three of these are associated with the patch (stiffener) centre-plane and the other three are associated with the sheet centre-plane The formulation of the element stiffness matrix is as follows The variation of the shear stresses τ_{zx} and τ_{zy} in the direction of the thickness of the sheet, adhesive and patch is shown in Figure 5-12(b) The shear stresses in the adhesive are assumed to be constant across its thickness, whereas they increase linearly from zero across the sheet and the patch Based on this assumed shear stress distribution, the shear stresses in the adhesive can be written as

$$\tau_{zx} = \frac{(u_p - u_s)}{R} \tag{5-20}$$

$$\tau_{zy} = \frac{(v_p - v_s)}{R} \tag{5-21}$$

where

$$R = \left(\frac{t_a}{G_a} + \frac{t_s}{4G_s} + \frac{3t_p}{8G_p} \right)$$

In Equations 5-20 and 5-21, the subscripts a, p, and s stand for adhesive, stiffener, and sheet respectively. u's and v's are x and y displacements as defined in Figure 5-12. G is the shear modulus. The average shear strain in the element is then given by

$$\varepsilon_{zx} = \frac{1}{3}\left[\frac{\left(u_p^1 - u_s^1\right)}{G_a \cdot R} + \frac{\left(u_p^2 - u_s^2\right)}{G_a \cdot R} + \frac{\left(u_p^3 - u_s^3\right)}{G_a \cdot R}\right] \tag{5-22}$$

and

$$\varepsilon_{zy} = \frac{1}{3}\left[\frac{\left(v_p^1 - v_s^1\right)}{G_a \cdot R} + \frac{\left(v_p^2 - v_s^2\right)}{G_a \cdot R} + \frac{\left(v_p^3 - v_s^3\right)}{G_a \cdot R}\right] \tag{5-23}$$

This can be written in matrix form as

$$\{\varepsilon\} = [B]\{\rho\}$$

where

$$\{\varepsilon\}^T = \{\varepsilon_{zx}\ \varepsilon_{zy}\}$$

$$[B] = \frac{1}{3G_aR}\begin{bmatrix} 1 & 0 & 1 & 0 & 1 & 0 & -1 & 0 & -1 & 0 & -1 & 0 \\ 0 & 1 & 0 & 1 & 0 & 1 & 0 & -1 & 0 & -1 & 0 & -1 \end{bmatrix}$$

$$\{\rho\}^T = \{u_p^1 v_p^1 u_p^2 v_p^2 u_p^3 v_p^3 u_s^1 v_s^1 u_s^2 v_s^2 u_s^3 v_s^3\}$$

The stress strain relationship is given by

$$\{\sigma\} = [D]\{\varepsilon\} \tag{5-24}$$

where

$$\{\sigma\}^T = \{\tau_{zx}\ \tau_{zy}\}$$

$$[D] = \begin{bmatrix} G_a & 0 \\ 0 & G_a \end{bmatrix}$$

The adhesive element stiffness matrix is obtained using the principal of virtual work as

$$[K]\{\rho\} = \{F\} \tag{5-25}$$

P516758.PDF [Page: 62 of 96]

where

$$K = \iint B^{\mathrm{T}} D B t_a \, \mathrm{d}x \, \mathrm{d}y$$

$$= B^{\mathrm{T}} D B V$$

V is the volume of the element

$$\{F\}^{\mathrm{T}} = \left\{ F_{\mathrm{px}}^1 F_{\mathrm{py}}^1 F_{\mathrm{px}}^2 F_{\mathrm{py}}^2 F_{\mathrm{px}}^3 F_{\mathrm{py}}^3 F_{\mathrm{sx}}^1 F_{\mathrm{sy}}^1 F_{\mathrm{sx}}^2 F_{\mathrm{sy}}^2 F_{\mathrm{sx}}^3 F_{\mathrm{sy}}^3 \right\}$$

The adhesive stiffness matrix is then coupled with the membrane stiffness matrices of the sheet and stiffener to form the combined stiffness matrix of the stiffener-adhesive-sheet composite element. The strain energy release rates are calculated using the following crack closure integral on the quarter point singularity elements that are used around the crack-tip

$$G_{\mathrm{I}} = \frac{v_4}{\Delta a}\left[F_{2y} + (1.5\pi - 4)F_{1y}\right] \tag{5-26}$$

$$G_{\mathrm{II}} = \frac{u_4}{\Delta a}\left[F_{2x} + (1.5\pi - 4)F_{1x}\right] \tag{5-27}$$

where G_{I} and G_{II} are the strain release rate for mode I and mode II loading, respectively, u_4 and v_4 are the opening displacements of the quarter points shown in Figure 5-13. F's are crack closure forces also shown in Figure 5-13. The stress intensity factors are then calculated using Equation 2-5, $G = K^2 / E$.

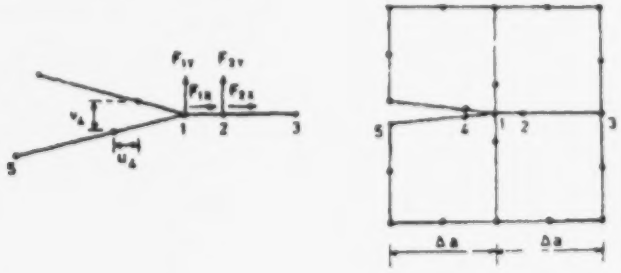

Figure 5-13 Forces and displacements associated with crack closure integral [13]

P516758.PDF [Page: 63 of 96]

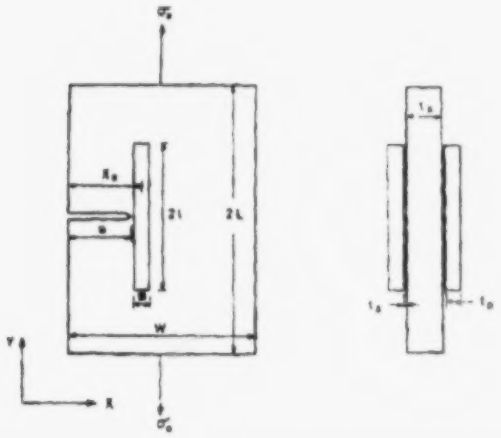

Figure 5-14 Edge crack-stiffened panel under mode I loading [13]

Using the triangular element, Sethuraman and Maiti [13] performed a parametric study on an edge crack-stiffened panel as shown in Figure 5-14 in addition to the problem presented in Section 5.2.3. In the case of the centre cracked-stiffened panel only a quarter of the panel is discretized, using 660 elements and 1640 nodes. In the case of the edge cracked-stiffened panel, half of the panel was discretized with the same number of elements and nodes. The longitudinal and transverse shear stresses developed in the adhesive, along its centre line were computed and compared to the analytical results in the case of mode I loading from Section 5.2.3. The transverse shear stress is plotted in Figure 5-15 and shows good agreement between analytical and finite element results. In addition the shear stresses in the case of the edge crack were shown to be lower than the case of centre crack under the same mode I loading. The same conclusion was reached regarding the influence of the stiffener location and adhesive thickness and shear modulus. That is the stiffener is in general the most effective when it is located close to the crack tip on the side opposite the ligament and increasing the shear modulus or reducing the thickness lowers the stress intensity factor of the stiffened structure.

P516758.PDF [Page: 64 of 96]

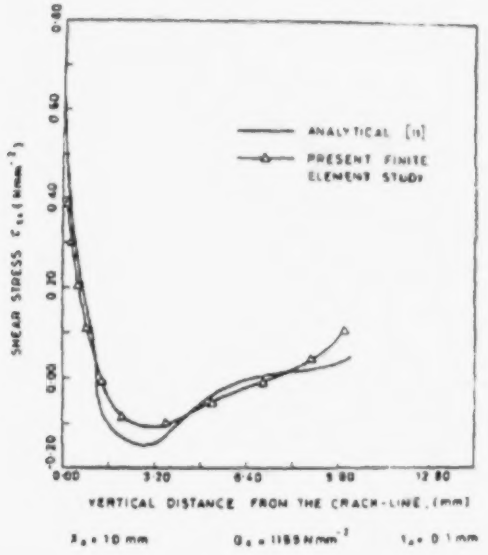

Figure 5-15 Variation of transverse shear stress along stiffener centre line for the centre crack problem under mode I loading [13]

5.3.2 Higher Order Element

In 1992, Maiti and Sethuraman [7] developed a higher order shear element for the analysis of doubly bonded cracked stiffened panels This element considers a parabolic variation of shear stresses in the thickness direction of the patch and the sheet and includes the energy due to shear deformation of the patch and the sheet in the element formulation It produces more accurate results than the constant strain triangular element discussed in the last section Maiti and Sethuraman [7] used this element for mixed-mode case studies to determine the most effective location and orientation of the stiffener.

The element geometry is shown in Figure 5-16 It shows the parabolic variation of the shear stress across the patch and sheet thickness The shear stress in the adhesive is again constant Figure 5-16(b) shows the overlay of two elements, one for the sheet and one for the patch Each node has two degrees of freedom, u and v, representing the x and y displacement respectively Although two elements are shown here, using only one element with four degrees of freedom associated with each node produces the same results This was done by Maiti and Sethuraman [7] when developing their program

P516758.PDF [Page 65 of 96]

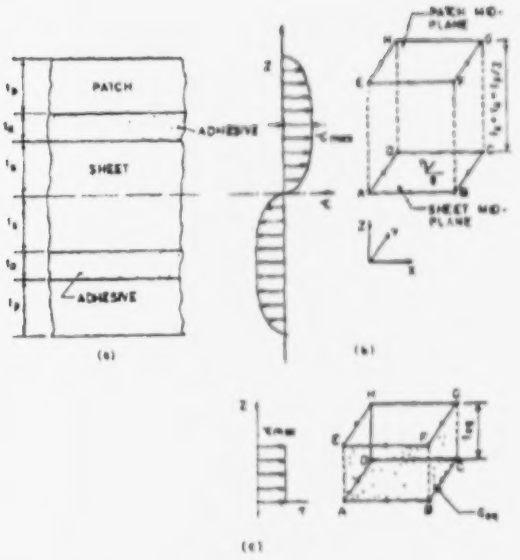

Figure 5-16 (a) Sheet-stiffener arrangement and shear stress distribution in the thickness direction (b) Overlay of two elements (c) Equivalent shear stress distribution and overlay arrangement [7]

The in-plane variations of the displacements are quadratic Therefore for the sheet

$$\begin{Bmatrix} u_s \\ v_s \end{Bmatrix} = \begin{bmatrix} N_1 & 0 & \cdots & N_8 & 0 \\ 0 & N_1 & \cdots & 0 & N_8 \end{bmatrix} \begin{Bmatrix} u_{s1} \\ v_{s1} \\ \vdots \\ u_{s8} \\ v_{s8} \end{Bmatrix} \tag{5-28}$$

where u_i's are the sheet displacement and N_i's are the displacement shape functions Equation 5-28 can be written in short as

$$\{u_s\} = [N]\{u_s\}_n \tag{5-29}$$

where $\{u_s\}_n$ is the element nodal displacements of the sheet Similarly, for the patch displacement u_p

$$\{u_p\} = [N]\{u_p\}_n \tag{5-30}$$

P516758.PDF [Page: 66 of 96]

The strain energy stored in the element is given by

$$U = U_m + U_s = \left(\frac{1}{2} \{u_s\}_n^T [K_s] \{u_s\}_n + \frac{1}{2} \{u_p\}_n^T [K_p] \{u_p\}_n \right) + \left(\frac{1}{2} \int_{A_e} \tau_{\max}^2 2 \left(\frac{t_p}{2G_p} + \frac{t_a}{G_a} + \frac{t_s}{2G_s} \right) dA \right) \tag{5-31}$$

where U_m and U_s is the strain energy due to in-plane or membrane deformation and due to shear deformation of the sheet, adhesive and the patch respectively. $[K_s]$ and $[K_p]$ are the membrane stiffness matrix of the sheet and the patch respectively. A_e is area of the element, and G_p, G_a, and G_s are the shear moduli

Figure 5-16(c) depicts an equivalent situation as in (b) having a constant shear stress of τ_{max}, a shear modulus of G_{eq}, and a thickness of t_{eq}. G_{eq} and t_{eq} are such that the shear deformation energy in (b) is equal that in (c). The stress-strain relationship and the shear deformation energy are given as

$$\frac{u_p - u_s}{t_{eq}} = \frac{\tau_{max}}{G_{eq}} \tag{5-32}$$

$$U_s = 2 \int_{A_e} \frac{\tau_{max}^2}{2G_{eq}} t_{eq} \, dA \tag{5-33}$$

Comparing U_s in Equations 5-31 and 5-33

$$\frac{t_{eq}}{G_{eq}} = \frac{t_p}{2G_p} + \frac{t_a}{G_a} + \frac{t_s}{2G_s} \tag{5-34}$$

From Equation 5-31, using Equation 5-32, one can write

$$U = \frac{1}{2} \{u_s\}_n^T [K_s] \{u_s\}_n + \frac{1}{2} \{u_p\}_n^T [K_p] \{u_p\}_n + \frac{1}{2} \{u_p\}_n - \{u_s\}_n^T [\bar{K}] \{u_p\}_n - \{u_s\}_n \tag{5-35}$$

where

$$[\bar{K}] = 2 \frac{G_{eq}}{t_{eq}} \int_{A_e} [N]^T [N] dA = \text{shear stiffness matrix} \tag{5-36}$$

Finally, Equation 5-35 can be rewritten as

PS16758.PDF [Page: 67 of 96]

$$U = \frac{1}{2}\{u\}_n^T [K]\{u\}_n \qquad (5\text{-}37)$$

where

$$\{u\} = \begin{Bmatrix} \{u_s\} \\ \{\} \\ \{u_p\} \end{Bmatrix}, \text{ and}$$

$$[K] = \begin{bmatrix} [K_s] + [\bar{K}] & -[\bar{K}] \\ -[\bar{K}] & [K_p] + [\bar{K}] \end{bmatrix} = \text{stiffness matrix for the composite element}$$

$[K]$ is of dimension 32 x 32

Maiti and Sethuraman [7] analyzed the centre crack-stiffened panel described in Section 5.2.3 using the higher order element to confirm its accuracy. One-quarter of the geometry was discretized into 176 elements. Variation of τ_{zy} along the stiffener centre line is plotted in Figure 5-17. It shows that the higher order element is more accurate than the constant shear strain element described in the last section.

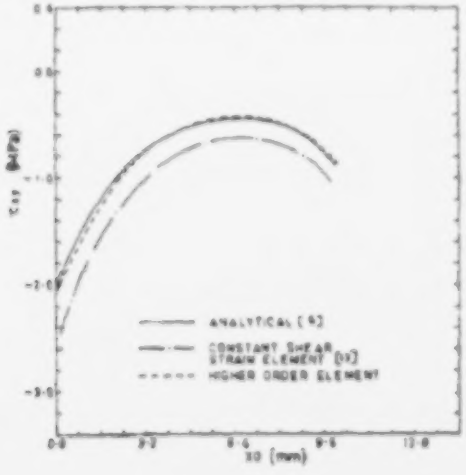

Figure 5-17 Comparison of variation of τ_{zy} along the stiffener centre line in the mode I problem [7]

Maiti and Sethuraman [7] then proceeded to determine the most effective location and orientation of the stiffener for the three edge crack loading cases shown in Figure 5-18 for three crack inclinations $\beta = 45°$, 60°, and 75°. The geometry was discretized into 165 quadratic elements and nine higher order elements. In each case, the direction of

P516758.PDF [Page: 68 of 96]

crack extension (θ_c) was determined by applying the criterion of maximum tangential stress of the linear elastic fracture mechanics. It is given by

$$K_I \sin\theta_c + K_{II}(3\cos\theta_c - 1) = 0 \qquad (5\text{-}38)$$

For each pair of K_I and K_{II} from each stiffener-crack-loading configuration, θ_c was determined and the maximum tangential stress $(\sigma_\theta)_{max}$ was calculated as:

$$\sqrt{2\pi r}(\sigma_\theta)_{max} = K_I \cos^3\frac{\theta_c}{2} - \frac{3}{2}K_{II}\cos\frac{\theta_c}{2}\sin\theta_c \qquad (5\text{-}39)$$

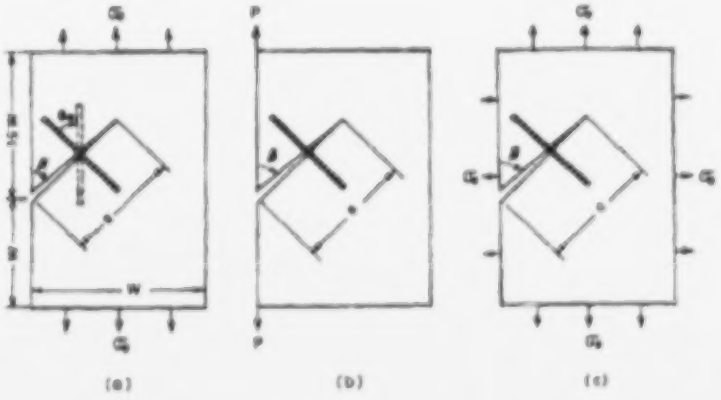

Figure 5-18 Three edge crack loading cases analyzed (a) Uniaxial load (b) Point load (c) Equibiaxial load [7]

The maximum tangential stress $(\sigma_\theta)_{max,0}$ in the unstiffened plate was also determined. The most effective location and/or orientation of the stiffener was then assumed to be the one which makes the ratio $(\sigma_\theta)_{max}/(\sigma_\theta)_{max,0}$ a minimum. Variation of $(\sigma_\theta)_{max}/(\sigma_\theta)_{max,0}$ with stiffener location for equibiaxial loading is plotted in Figure 5-19. The effect of the stiffener orientation was then examined by rotating the stiffener about a fixed location. Variation of $(\sigma_\theta)_{max}/(\sigma_\theta)_{max,0}$ with stiffener orientation for equibiaxial loading is plotted in Figure 5-20. From the results obtained, Maiti and Sethuraman concluded that "in the cases where K_I dominates, placing the stiffener close to the centre of the crack and perpendicular to the direction of initial crack extension in the unstiffened panel gives the maximum advantage. In the cases where K_{II} is comparable to K_I, there is

P516753.PDF [Page: 69 of 96]

no stiffener orientation which makes the tangential stress a minimum, but there is a position close to the centre of the crack and an orientation close to the crack-normal position for which K_I has a minimum " [7]

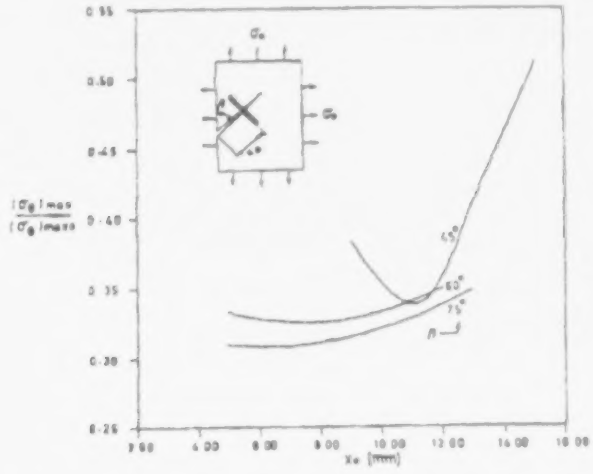

Figure 5-19 Variation of $(\sigma_\theta)_{max}/(\sigma_\theta)_{max0}$ with stiffener location X_o for equibiaxial loading [7]

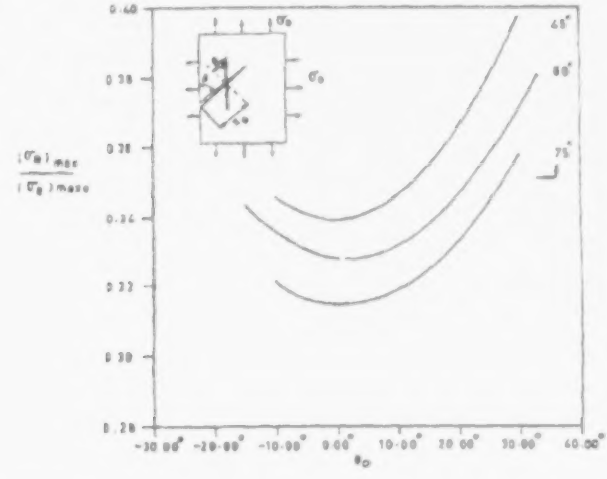

Figure 5-20 Variation of $(\sigma_\theta)_{max}/(\sigma_\theta)_{max0}$ with stiffener orientation θ_o for equibiaxial loading [7]

5.4 Boundary Element Method

In many solid mechanics problems, the boundary conditions on the surface of the body is specified by either the tractions or the displacements, where one quantity depends

P516758.PDF [Page: 70 of 96]

on the other In other words, it is possible to solve for the tractions at a point on the surface when the displacements are known and vice versa The boundary element method is one such technique for solving for the unknown tractions and displacements on the surface It is based on Betti's reciprocal theorem, which can be stated as "The virtual work U_{IB} done by a system of forces ΣP_B that undergo a displacement caused by a system of forces ΣP_A is equal to the virtual work U_{BA} caused by the forces ΣP_A when the structure deforms due to the system of forces ΣP_B"[4] In terms of surface tractions and displacments, Betti's theorem can be stated as follows

$$\int_S T_i^{(1)} u_i^{(2)} \, dS = \int_S T_i^{(2)} u_i^{(1)} \, dS \tag{5-40}$$

where T_i and u_i are components of the traction and displacement vectors, respectively, and the superscripts denote loadings (1) and (2)

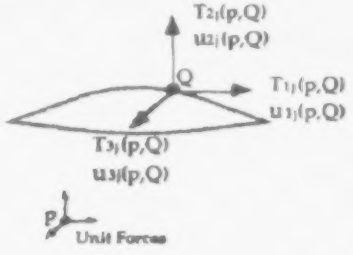

Figure 5-21 Reference boundary conditions for a boundary integral element problem [1]

A reference load can be considered as a unit force applied at an interior point p in each of three coordinate directions as shown in Figure 5-21 A unit force in any one of the directions may produce displacements and tractions at Q in all three coordinate directions Therefore, the resulting displacements and tractions at Q, $u_{ij}(p,Q)$ and $T_{ij}(p,Q)$ are second-order tensors and their values have closed-form solutions for several cases Applying the Betti's reciprocal theorem to this situation gives

$$u_i(p) = -\int_S T_{ij}(p,Q) u_j(Q) \, dS + \int_S u_{ij}(p,Q) T_j(Q) \, dS \tag{5-41}$$

P516758.PDF [Page: 71 of 96]

where $u_i(p)$ is the displacement vector at the interior point p and $u_i(Q)$ and $T_i(Q)$ are displacements and tractions at the boundary point Q corresponding to the loading of interest. At a given point Q on the boundary, either traction or displacement is prescribed, and the other quantity can be determined accordingly. If p approaches a point P on the surface, then for a smooth surface, Equation 5-41 becomes

$$\frac{1}{2}u_i(P) + \int_S T_{ij}(P,Q)u_j(Q)\,dS = \int_S u_{ij}(P,Q)T_j(Q)\,dS \tag{5-42}$$

Equation 5-42 represents a set of integral constraint equations that relate surface displacements to surface tractions. Rather than integrating the equations directly, the surface can be subdivided into segments (elements), and Equation 5-42 is then approximated by a system of algebraic equations. If u_i and T_i are assumed to vary linearly between nodal points on the surface, then Equation 5-42 can be written as

$$\left[\frac{1}{2}\delta_{ij}\right] + \left[\Delta T_{ij}\right]\{u_j\} = \left[\Delta u_{ij}\right]\{T_j\} \tag{5-43}$$

where δ_{ij} is the Kronecker delta with the property that $\delta_{ij} = 0$ for $i \neq j$ and that $\delta_{ij} = 1$ for $i = j$. If n is the number of nodes, then for a three-dimensional problem Equation 5-43 represents a set of $3n$ equations since there are three degrees of freedom for every node points. When all of the boundary quantities are known, the internal displacement of the body can be determined from Equation 5-41.

Since the boundary elements have one less dimension than the body being analyzed (for example the boundary of a two-dimensional problem is surrounded by one-dimensional elements), the boundary element method is best suited for problems where the boundary quantities are of primary interest. However, when solving for internal field quantities, the finite element method is a more efficient choice.

5.4.1 Application to Cracked Stiffened Panels

The boundary element method is a popular numerical technique for solving crack problems since it has the ability of reducing the dimensionality of the problem such that the high stress gradients near the crack tip can be modeled more efficiently with one less

P516758.PDF [Page: 72 of 96]

dimension It has also been shown that the method produces more accurate stress intensity factors than the finite element method The dual boundary element method, which uses the displacement equation when collocating at one crack surface and the dual traction equation when collocating at the other crack surface, is a variation of the boundary element method It is the method of choice for Salgado and Aliabadi [11] on their investigation on crack growth in cracked stiffened panels

The boundary integral displacement equation, for a source point x' at the boundary Γ of a finite sheet is given by

$$c_{ij}(x')u_j(x') + \oint_\Gamma T_{ij}(x',x)u_j(x)\,d\Gamma(x) = \int_\Gamma U_{ij}(x',x)t_j(x)\,d\Gamma(x) + \iint_\Omega U_{ij}(x',X)b_j(X)\,d\Omega(X) \tag{5-44}$$

where $T_{ij}(x',x)$ and $U_{ij}(x',x)$ are the Kelvin traction and displacement fundamental solutions, respectively, $u_j(x)$ and $t_j(x)$ are displacement and tractions at boundary field points x, $b_j(X)$ are body forces acting at field points X inside the domain Ω, $\oint$ stands for principal value integral and c_{ij} is a coefficient that can be determined by rigid body movement considerations Equation 5-44 is similar to Equation 5-42 except for the incorporation of the body force term in the former

The corresponding traction boundary integral equation is obtained by differentiation of Equation 5-44, application of Hooke's law and multiplication by the outward normal

$$\begin{aligned}\frac{1}{2}t_j(x') + n_i(x')\oint_\Gamma S_{ijk}(x',x)u_k(x)\,d\Gamma(x) &= n_i(x')\int_\Gamma D_{ijk}(x',x)t_k(x)\,d\Gamma(x) \\ &+ \iint_\Omega D_{ijk}(x',X)b_k(X)\,d\Omega(X)\end{aligned} \tag{5-45}$$

where $S_{ijk}(x',x)$ and $D_{ijk}(x',x)$ contain derivatives of $T_{ij}(x',x)$ and $U_{ij}(x',x)$, respectively and $n_i(x')$ denotes the i-th component of the unit outward normal to the boundary at the source point x'

If the body forces are confined to n straight lines inside the whole domain instead of being distributed over it, then the double integrals in Equation 5-44 and 5-45 reduce to

P516758.PDF [Page: 73 of 96]

line integrals over the body forces loci. The dual boundary element method then proceeds by discretizing the boundary Γ and the body forces loci L_n into a set of elements. A system of simultaneous linear equations is obtained by taking the collocation point to lie at each of the boundary element nodes and using Equation 5-44. If a crack is present, Equation 5-45 is used instead when collocating at one of the crack surfaces. From the set of equations the unknown surface tractions and displacements are determined.

The stiffener was modeled subject to the following set of in-plane loads as shown in Figure 5-22: distributed loads, concentrated loads, and end moments. The relative end displacements in the stiffeners' transverse and longitudinal directions were expressed in terms of the applied loads. The interaction forces between the stiffener and the sheet were treated in the boundary integral equations as the body forces distributed along lines. The condition that the displacements of the sheet and the stiffener at node points are compatible with the shear deformation of the adhesive layer connecting them was enforced, where the relative displacement of the sheet's internal points at the attachment was determined from Equation 5-44 with line integrals. The unknown boundary displacements, boundary tractions, interaction forces, and the stiffeners rigid body rotation coefficient were determined from the set of displacement compatibility equations and the stiffener equilibrium equations. The stress intensity factors were then computed from the J-integral, which requires the calculation of stresses and displacement derivatives at internal points using Equations 5-44 and 5-45 with line integrals.

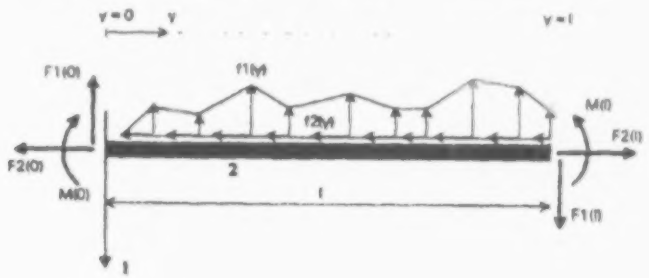

Figure 5-22 Isolated stiffener subjected to a set of in-plane loads [11]

Salgado and Aliabadi [11] analyzed both continuously and discretely attached stiffeners. For the discretely attached case, the interaction forces were considered

P516758.PDF [Page: 74 of 96]

concentrated at points, corresponding to the fastener locations and the integrals over the stiffener elements reduced to summations For all the cases the external boundaries and stiffeners loci are discretized using continuous, isoparametric, quadratic elements The crack boundaries were discretized with discontinuous elements The *J*-integral path in calculating the stress intensity factor was a circle centred at the crack tip with the radius being half the crack tip element size Partial debonding or rivet failure was implemented by imposing zero interaction forces in the system of equations

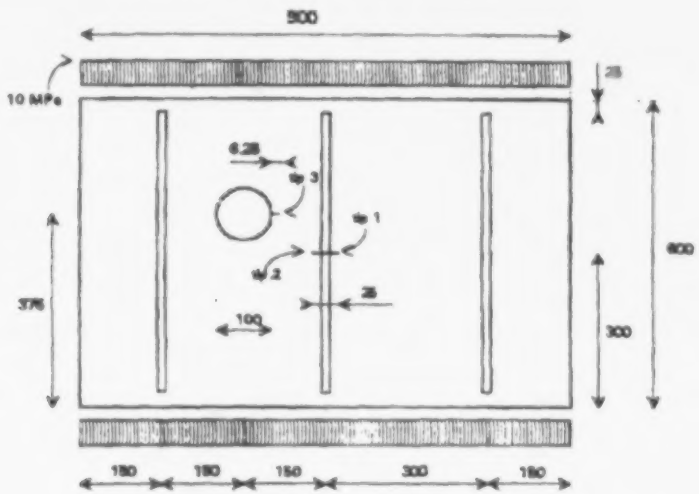

Figure 5-23 Cracked panel reinforced by riveted stiffeners [11]

Salgado and Aliabadi [11] first analyzed the case of a crack symmetrical about a stiffener and the case of a crack near a stiffener In both cases both continuously attached and discretely attached stiffeners were used The calculated crack tip stress intensity factors for all cases were found agree with published results A multiple-fatigue-crack growth analysis was then performed on the cracked panel with a broken central stiffener as shown in Figure 5-23 In the analysis the direction of crack growth was assumed to be in the direction perpendicular to the maximum principal stress direction at the crack tip. The Paris law was used to calculate the crack increment size The boundary element mesh and the crack growth paths are presented in Figure 5-24 The crack growth diagram is shown in Figure 5-25

P516758.PDF [Page: 75 of 96]

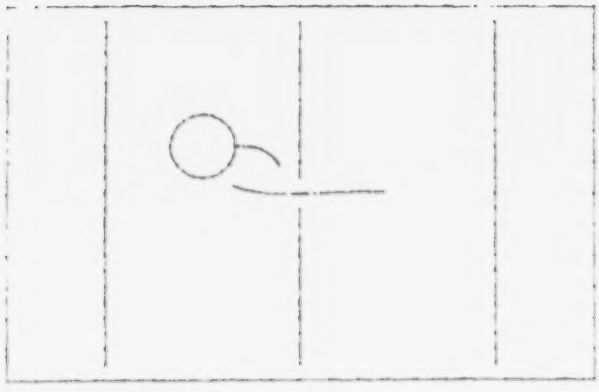

Figure 5-24 Boundary element mesh and crack paths after ten crack increments [11]

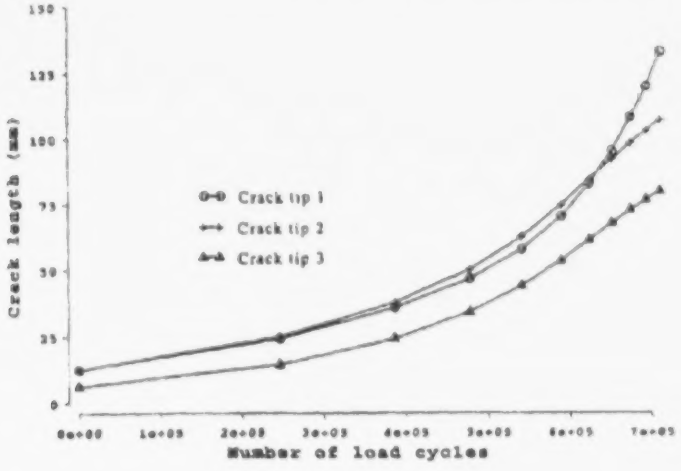

Figure 5-25 Crack growth diagram [11]

5.4.2 Dynamic Effects of Breaking Stiffeners

When a stiffener suddenly breaks, the load it is previously carrying is transferred to the sheet, causing an increase in stress intensity factor for the crack. The magnitude of this increase depends on many factors such as the relative stiffness of the stiffener and sheet, the length of the crack and the type of stiffener attachment. Rooke *et al* [9] considered the dynamic effects of breaking stiffeners by modeling a broken stiffener as an intact stiffener plus an opening force acting on the crack faces. The boundary element method was chosen for the stress analysis.

P516758.PDF [Page: 76 of 96]

Figure 5-26 Broken stiffener equals unbroken stiffener plus "opening" force *P* [9]

The broken stiffener was modeled by the superposition of an intact stiffener plus an opening force P' acting on the crack faces as shown in Figure 5-26. The magnitude of P' is determined from the difference between the steady-state values of the stress intensity factors for the broken and unbroken state. The effect of sudden breaking of the stiffener can then be simulated by suddenly imposing P' on the crack faces. The dynamic stress intensity factor $K_b^{sf}(t)$ for the broken stiffener configuration is then the sum of the static unbroken case, K_u^s, and $K^{sf}(t)$, which is the dynamic stress intensity factor for the force P' acting on the crack surfaces. Thus,

$$K_b^{sf}(t) = K_u^s + K^{sf}(t) \tag{5-46}$$

The static K_u^s is known for many simple configurations and for their dynamic analysis, Rooke *et al* [9] considered a simple case of a single stiffener symmetrically located across a single crack in an infinite sheet subjected to a remote uniform tensile stress σ.

The distribution of P' on the crack faces is not known and it can be represented as a pressure $p(x)$ on the crack faces such that the total force is equal to P'. Four different distributions of $p(x)$ were studied by Rooke *et al* to investigate the effects of force distribution on the dynamic stress intensity factor. The distributions considered were constant pressure (p_1), linearly varying pressure (p_2), and two quadratically varying pressures (p_3 and p_4). They are shown in Figure 5-27 and are assumed to act over a distance of $2l$ such that $l \le a$.

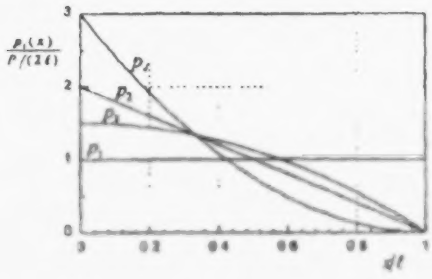

Figure 5-27 Pressure distribution on half the crack [9]

The stress analysis of the dynamically loaded crack was obtained using the boundary element method. The model, as shown in Figure 5-28, contained 64 boundary elements and 54 domain points with four elements on each surface of the crack for all the calculations, except the smallest value of $l = 0.4a$. In that case, two extra elements were included next to the crack on the boundary $x = 0$ to improve accuracy. The dynamic stress intensity factors were obtained from the dynamic J-integrals. The static stress intensity factors were obtained using the Green's function.

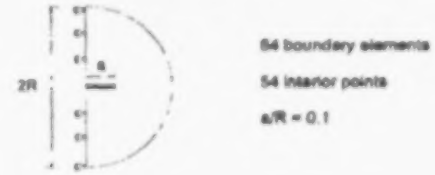

Figure 5-28 Boundary element model of crack configuration [9]

The obtain the dynamic effects, the pressure $p(x)$ is applied to the crack face using the Heaviside step-function $H(t)$

$$p_i(x,t) = p_i(x)H(t), \quad i = 1 \ldots 4, \tag{5-47}$$

where $H(t)$ is defined as

$$\begin{aligned} H(t) &= 1, \quad t \geq 0 \\ H(t) &= 0, \quad t < 0 \end{aligned} \tag{5-48}$$

Equation 5-47 has the effect of applying the pressure instantaneously at $t = 0$. This corresponds to a stiffener breaking at $t = 0$.

The results for the dynamic stress intensity factor $K^{d}(t)$ were normalized with respect to K_p, where K_p is the value of the static stress intensity with the opening force P acting at the centre of the crack, and are plotted in Figure 5-29 as a function of time $K^{d}(t)$ were calculated for several values of λ for each stress distribution, where $\lambda = l/a$. The plots show that the stress intensity factors were not very dependent on λ for all the distribution except the constant stress, where the normalized $K^{d}(t)$ is significantly higher for $\lambda = 1.0$. For all other cases, the peak $K^{d}(t)$ values occurred at about the same time interval after the loads are applied and were all of the same magnitude. For all the stress distributions, except for the constant stress at $\lambda = 1.0$, the peak values are between 45 to 60% greater than K_p for the values of λ considered. However, if the peak dynamic stress intensity factor, K^{dl}_{peak}, is normalized with respect to the static stress intensity factor at the given l instead of the limiting value K_p, then a different trend was observed. In this case, the distribution, p_1 showed the lowest normalized peak values while p_4 showed the highest for all values of λ considered. Rooke *et al* [9] concluded that the more the stiffener load is concentrated at the centre of the crack, the greater the increase over the static stress intensity factor when the stiffener breaks.

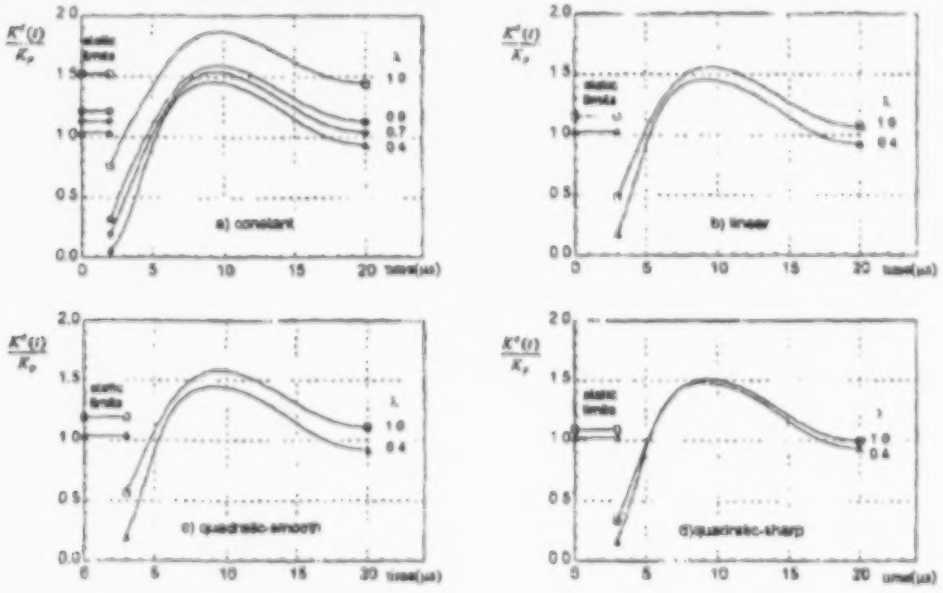

Figure 5-29 Dynamic stress intensity factors for various crack-face loadings [9]

P516758.PDF [Page: 79 of 96]

Rooke *et al* [9] then proceeded to calculate the dynamic stress intensity factor $K_b^{sl}(t)$ for the configuration with a broken stiffener as given in Equation 5-46. They assumed that the values of the static stress intensity factor, K_s, caused by the applied pressures are equal to the difference between the static stress intensity factors for the broken and unbroken stiffener cases. Normalizing with respect to $K_0 = \sigma\sqrt{\pi a}$ yields,

$$\frac{K_s}{K_0} = \frac{K_b^s}{K_0} - \frac{K_u^s}{K_0} \tag{5-49}$$

K_b^s and K_u^{sl} are known for many geometry

The dynamic stress intensity factor $K^{sl}(t)$ determined before can be written as

$$\frac{K^{sl}(t)}{K_0} = \frac{K^{sl}(t)}{K_s}\cdot\frac{K_s}{K_0} \tag{5-50}$$

Substituting Equations 5-49 and 5-50 into 5-46 yields

$$\frac{K_b^{sl}(t)}{K_0} = \frac{K_u^s}{K_0} + \frac{K^{sl}(t)}{K_s}\cdot\left[\frac{K_b^s}{K_0} - \frac{K_u^s}{K_0}\right] \tag{5-51}$$

The peak value $\left(K_b^{sl}/K_0\right)_{peak}$ is obtained when $K^{sl}(t) = K_{peak}^{sl}$ as determined before

The values of K_b^s/K_0, K_u^{sl}/K_0, and $\left(K_b^{sl}/K_0\right)_{peak}$ are plotted in Figure 5-30 against the normalized crack length a/L, where L is defined as

$$L = \frac{AE_{st}}{2tE_{sh}} \tag{5-52}$$

where t is the sheet thickness, A is the stiffener cross-sectional area and E_{sh} and E_{st} are the Young's modulus of the sheet and stiffener, respectively. It can again be seen from the figure that the more the load is restricted to the centre of the crack (smaller λ) the greater the value of the peak dynamic stress intensity factor. However, the effect is not great except for the constant distribution. The magnitude of the dynamic overshoot D is plotted against the normalized crack length in Figure 5-31 for p_1 and p_4 pressure

P516758.PDF [Page: 80 of 96]

distributions D represents the difference between the peak dynamic stress intensity factor and the static value and is defined as

$$D = \frac{\left(K_h^d\right)_{peak} - K_h^s}{K_h^s} \cdot 100\% \tag{5.53}$$

In the figure the shaded area represents the D values for λ between 0.4 to 1.0 with the upper limit at $\lambda = 0.4$. Rooke *et al* concluded from the figure that the largest overshoot occurs at the smallest crack length and the most loads concentrated at the centre of the crack.

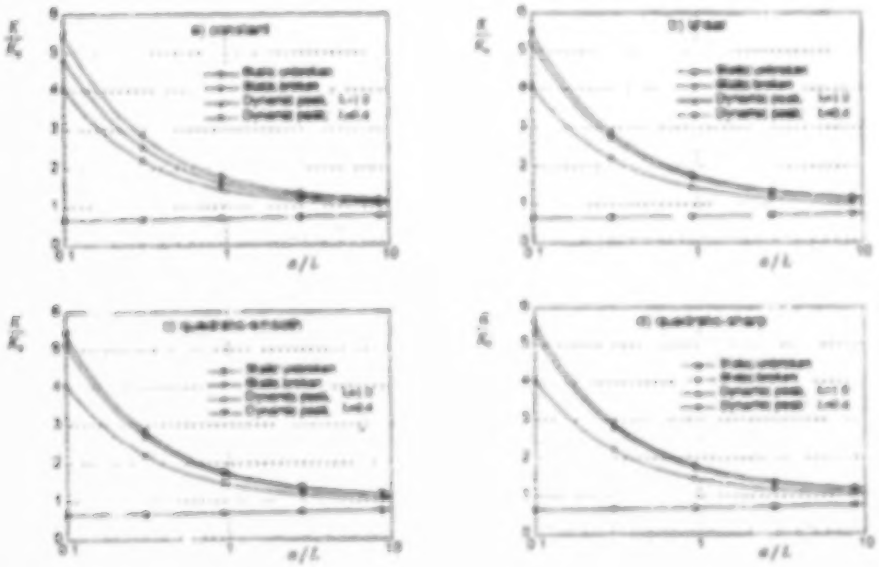

Figure 5-30 Static and peak dynamic stress intensity factors for a crack in a stiffened sheet [9]

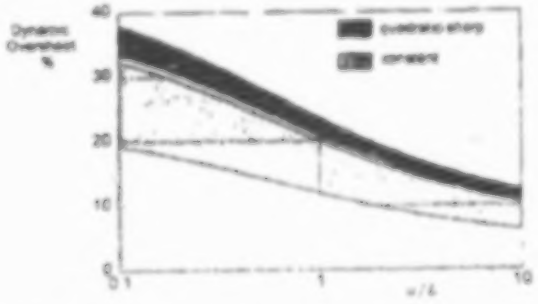

Figure 5-31 Dynamic overshoot of the stress intensity factor after a stiffener breaks [9]

5.5 *Finite Difference Method*

The finite difference method is an effective numerical method for solving differential equations. The method is based on replacing differentiation by an approximating difference formula which involves only simple arithmetic operations. For example the central difference formula for approximating the first derivative of a function $f(t)$ with respect to t is given by

$$\frac{\mathrm{d}\, f(t)}{\mathrm{d}t} = \frac{f(x+\Delta t) - f(x-\Delta t)}{2\Delta t} \tag{5-54}$$

The approximation becomes more and more accurate as Δt approaches zero. When analyzing a structure with the finite difference method, the method requires the domain to be replaced by a mesh if the derivatives in the governing differential equation involved are with respect to the geometry. At each grid point, each term in the derivatives is replaced by a difference formula which may include the values of at that and neighbouring grid points. After the boundary conditions are imposed, a set of algebraic equations is then obtained from the value of the function of interest at each grid point is obtained. The finite difference method is ideal for solving dynamic problems in which the equation of motion is in the form of a partial differential equation. This method has been applied to dynamic fracture analysis of stiffened structures by several investigators and some of their results are presented below.

5.5.1 Basic Equations in Dynamic Fracture Analysis

The following finite difference formulation for the two-dimensional dynamic fracture problems is given by Liu *et al.* [5] and Wang *et al.* [14]. The equations of motion are.

$$\begin{aligned} \rho \frac{\partial^2 U}{\partial t^2} &= \frac{\partial \sigma_{xx}}{\partial x} + \frac{\partial \tau_{xy}}{\partial y} + X \\ \rho \frac{\partial^2 V}{\partial t^2} &= \frac{\partial \tau_{xy}}{\partial x} + \frac{\partial \sigma_{yy}}{\partial y} + Y \end{aligned} \tag{5-55}$$

where ρ is the mass density of the elastic material, and X and Y the body forces

P516758.PDF [Page: 82 of 96]

The stress-strain relations are

$$\sigma_{xx} = (\lambda + 2\mu)\frac{\partial U}{\partial x} + \lambda \frac{\partial V}{\partial y}$$

$$\sigma_{yy} = (\lambda + 2\mu)\frac{\partial V}{\partial y} + \lambda \frac{\partial U}{\partial x} \qquad (5\text{-}56)$$

$$\tau_{xy} = \mu\left(\frac{\partial U}{\partial y} + \frac{\partial V}{\partial x}\right)$$

where λ and μ are the Lamé constants

From Equations 5-55 and 5-56, the wave equations can be obtained as

$$\theta\frac{\partial U}{\partial t} + \frac{\partial^2 U}{\partial t^2} = c_1^2\frac{\partial^2 U}{\partial x^2} + \left(c_1^2 - c_2^2\right)\frac{\partial^2 V}{\partial x \partial y} + c_2^2\frac{\partial^2 U}{\partial y^2} + X$$

$$\theta\frac{\partial V}{\partial t} + \frac{\partial^2 V}{\partial t^2} = c_2^2\frac{\partial^2 V}{\partial x^2} + \left(c_1^2 - c_2^2\right)\frac{\partial^2 U}{\partial x \partial y} + c_1^2\frac{\partial^2 V}{\partial y^2} + Y \qquad (5\text{-}57)$$

where the damping terms, $\theta(\partial U/\partial t)$ and $\theta(\partial V/\partial t)$, are added to Equation 5-55 and c_1 and c_2 are the axial and shear wave velocities given by

$$c_1^2 = \frac{\lambda + 2\mu}{\rho}, \quad c_2^2 = \frac{\mu}{\rho} \qquad (5\text{-}58)$$

Equation 5-57 is the basis for the dynamic fracture analysis of a stiffened panel performed by Liu *et al* [5] and Wang *et al* [14]. Using a mesh size of h and a time increment of τ, for a panel subjected to a uniform tensile stress in the y direction, the central difference formulae of the wave equation are

$$U_{i,j}(t+\tau) = \frac{1}{1+0.5\tau\theta}\left\{2U_{i,j}(t) - (1-0.5\tau\theta)U_{i,j}(t-\tau) + \left(\frac{c_1\tau}{h}\right)^2\left(U_{i+1,j}(t)\right.\right.$$

$$\left. - 2U_{i,j}(t) + U_{i-1,j}(t)\right) + \left(c_1^2 - c_2^2\right)\left(\frac{\tau}{2h}\right)^2\left(V_{i+1,j+1}(t) - V_{i+1,j-1}(t)\right.$$

$$\left.\left. - V_{i-1,j+1}(t) + V_{i-1,j-1}(t)\right) + \left(\frac{c_2\tau}{h}\right)^2\left(U_{i,j+1}(t) - 2U_{i,j}(t) + U_{i,j-1}(t)\right)\right\}$$

PS16758.PDF [Page: 83 of 96]

$$U_{i,j}(t+\tau)=\frac{1}{1+0.5\tau\theta}\left\{2U_{i,j}(t)-(1-0.5\tau\theta)U_{i,j}(t-\tau)+\left(\frac{C_2\tau}{h}\right)^2\left(U_{i+1,j}(t)\right.\right.$$

$$-2U_{i,j}(t)+U_{i-1,j}(t))+\left(C_1^2-C_2^2\right)\left(\frac{\tau}{2h}\right)^2(U_{i+1,j+1}(t)-U_{i+1,j-1}(t)$$

$$\left.\left.-U_{i-1,j+1}(t)+U_{i-1,j-1}(t))+\left(\frac{C_2\tau}{h}\right)^2(U_{i,j+1}(t)-2U_{i,j}(t)+U_{i,j-1}(t))+\tau^2Y\right\}\right.$$

$$i=2,3,\ldots,(N-1)$$
$$j=2,3,\ldots,(M-1) \qquad (5\text{-}59)$$

where N and M are the line numbers in the x and y directions of the mesh and Y is replaced by a compulsive condition in the analysis of Liu *et al* [5]

5.5.2 Analysis by Liu *et al*

Liu *et al* [5] performed a dynamic fracture analysis of a stiffened panel with a central crack as shown in Figure 5-32. Because of symmetry, only a quarter of the panel was meshed as shown in Figure 5-33. By imposing the sheet-stiffener displacement compatibility at the attachment locations, the compulsive condition in finite difference form at the Kth fastener position is derived as follows and applied at $x = I$, where the stiffener is attached

$$U_{N,K}=U_{N-1,K}-0.5\left[\left(U_{N-1,K+1}-U_{N-1,K-1}\right)-A_sE_s/(\mu D_s)\right]\left[0.5\left(U_{N-1,K+1}-U_{N-1,K-1}\right)\right.$$

$$\left.-h\sum_{j=K+1}^{n}Q_j/(A_sE_s)\right] \qquad (5\text{-}60)$$

where A_s and E_s are the cross-sectional area and the Young's modulus of the stiffener, D_s is the diameter of the fastener, n is the number of fasteners per stiffener, and Q_j is the load transferred by the jth stiffener. The following boundary conditions were also applied to the central difference formulae

P516753.PDF (Page: 84 of 96)

$$
\begin{aligned}
&\sigma_{yy} = 0, \quad \tau_{xy} = 0 \quad \text{when } y = 0, \quad 0 \le x \le a \\
&U = 0, \quad \tau_{xy} = 0 \quad \text{when } y = 0, \quad a < x \le L \\
&\sigma_{yy} = \sigma, \quad \tau_{xy} = 0 \quad \text{when } y = H, \quad 0 \le x \le L \\
&U = 0, \quad \tau_{xy} = 0 \quad \text{when } x = 0, \quad 0 \le y \le H \\
&\sigma_{xx} = 0, \quad \tau_{xy} = 0 \quad \text{when } x = L, \quad 0 \le y \le H
\end{aligned}
\tag{5-61}
$$

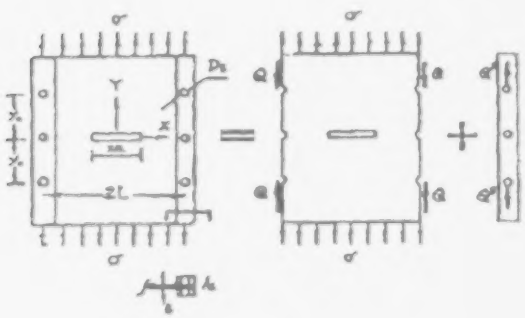

Figure 5-32 Resolution of a stiffened panel [5]

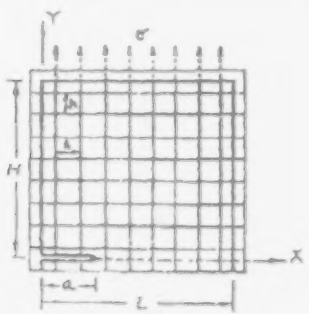

Figure 5-33 Calculation mesh for quarter of panel [5]

The wave equations can then be solved at each grid point by imposing the boundary and compulsive conditions on the central difference formulae The stress at a half h in front of the crack tip, $\sigma_i(t)$, was then compared with the critical fracture stress, $\sigma_c(t)$, in the following crack propagation criterion "If $\sigma_1(t) \ge \sigma_c(t)$, then the crack will be propagating, conversely, if $\sigma_1(t) \le \sigma_c(t)$, it will not be propagating If $\sigma_1(t) \le \sigma_c(t)$ in enough time steps, the crack can be considered as in arrest "[5] Figure 5-34 compares the crack propagation velocity in the stiffened panel with the finite plate It can be seen that the crack velocity for the stiffened panel is less than that for the finite

P516758.PDF [Page: 85 of 96]

plate. Figure 5-35 shows the effect of the stiffener's Young's modulus E_s on crack velocity. It can be seen that the crack velocity decreases with E_s. In the case shown in the figure, the crack was arrested when $a/h = 20$ for the case of $E_s/E = 1.88$.

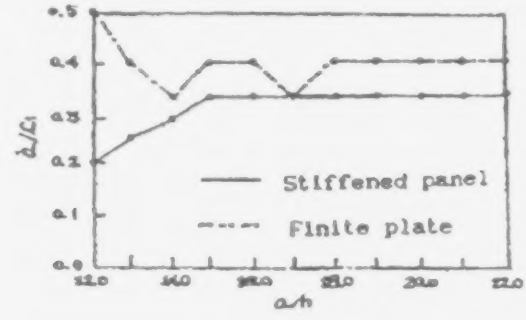

Figure 5-34 Comparison of crack velocity [5]

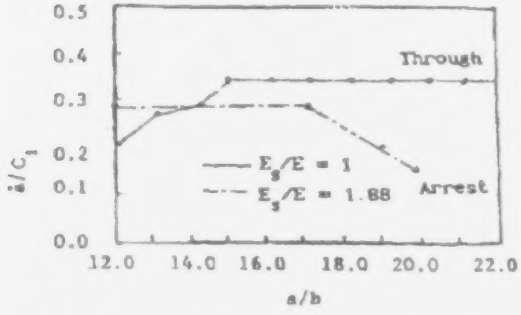

Figure 5-35 Influence of E_s/E on velocity [5]

5.5.3 Analysis by Wang *et al*

Wang *et al* [14] investigated the effects of different cross-sectional areas and different positions of the stiffener in a stiffened panel with an edge crack shown in Figure 5-36 using the finite difference method. Because of symmetry, only half of the panel was meshed as shown in Figure 5-37.

P516758.PDF [Page: 86 of 96]

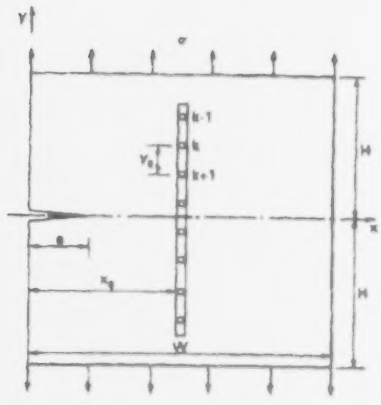

Figure 5-36 A stiffened panel with an edge crack [14]

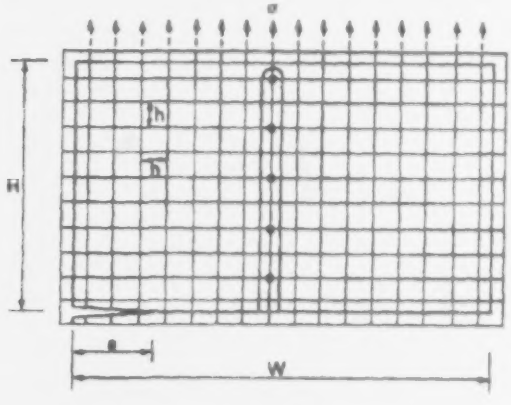

Figure 5-37 Calculation mesh for half of panel [14]

The panel-stiffener interaction was accounted for by considering the free body diagram of a section of the stiffener as shown in Figure 5-38, where Q_k is the force transmitted from the panel to the stiffener through the kth rivet and $T_{k-1}^{\prime}$ and $T_k^{\prime}$ are the tensile force from the upper and lower part of the stiffener respectively. If Q_k is assumed to act uniformly along the horizontal diameter of the rivet, then the body force Y acting on the panel is given by

$$Y = \frac{Q_k^{\prime}}{tD_{\prime}} \tag{5-62}$$

P516758.PDF [Page: 87 of 96]

where $Q_k^{(s)} = -Q_k$ is the reaction force transmitted from the stiffener to the panel, t is the thickness of the panel, and D_r is the diameter of the rivet hole. From Figure 5-38, equilibrium of forces gives

$$Q_k = T_k^{(s)} - T_{k-1}^{(s)} \tag{5-63}$$

Figure 5-38 Equilibrium of the stiffener [14]

The forces $T_{k-1}^{(s)}$ and $T_k^{(s)}$ can be determined from the familiar mechanics equation for axial displacement, $\Delta = PL/AE$. That is

$$T_{k-1}^{(s)} = \frac{V_{k-1}^{(s)} - V_k^{(s)}}{y_0} A_s E_s \tag{5-64}$$

where $V_k^{(s)}$ is the y-direction displacement at the rivet k, y_0 is the distance between two rivets, and A_s and E_s are the cross-sectional area and the Young's modulus of the stiffener respectively. $T_k^{(s)}$ is determined in the same way by $V_k^{(s)}$ and $V_{k-1}^{(s)}$.

By incorporating the body force Y into the wave equation and imposing the boundary conditions below, the displacement of each grid point can be solved, from which the stresses and stress intensity factor can be determined

$$\begin{aligned}
&\sigma_{yy} = 0, \quad \tau_{xy} = 0 \quad \text{when } y = 0, \quad 0 \le x \le a \\
&V = 0, \quad \tau_{xy} = 0 \quad \text{when } y = 0, \quad a < x \le W \\
&\sigma_{yy} = \sigma, \quad \tau_{xy} = 0 \quad \text{when } y = H, \quad 0 \le x \le W \\
&\sigma_{xx} = 0, \quad \tau_{xy} = 0 \quad \text{when } x = 0, \quad 0 \le y \le H \\
&\sigma_{xx} = 0, \quad \tau_{xy} = 0 \quad \text{when } x = W, \quad 0 \le y \le H
\end{aligned} \tag{5-65}$$

P516758.PDF [Page: 88 of 96]

The same crack propagation criterion was used as in Liu *et al* [5] In this case the crack tip stress intensity factor at each time step was compared to the dynamic fracture toughness, K_{ID}, given by

$$K_{ID} = \frac{K_{I1}}{1-(a/V_f)^m} \tag{5-66}$$

where K_{I1} denotes the minimum value of K_{ID} with respect to crack speed a, V_f corresponds to a limiting crack speed, and m is a dimensionless shape factor To represent 4340 steel data, V_f = 1100 m/sec and m = 2 was chosen

The edge crack-stiffened panel shown in Figure 5-36 was analyzed with an initial crack length of 0 14 m The influence of the cross-sectional area of the stiffener, A_s, was investigated first The variation of the static stress intensity factor, K_I, with A_s is plotted in Figure 5-39 It can be seen that K_I decreases as A_s increases as more load is transferred to a larger stiffener The crack propagation velocity, V, is plotted against the crack propagation length, a, in Figure 5-40 for various values of A_s It can be seen that V decreases as A_s increases Crack propagation was arrested for $A_s \geq 2\times10^{-3}\,\mathrm{m}^2$ For $A_s \geq 5\times10^{-3}\,\mathrm{m}^2$, the crack would not propagate at all

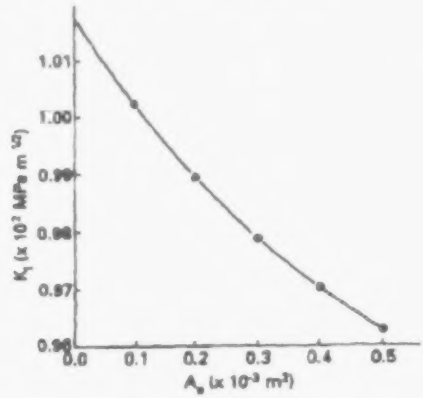

Figure 5-39 Static K_I variation with A_s (X_0 = 0.18 m) [14]

P516758.PDF [Page: 89 of 96]

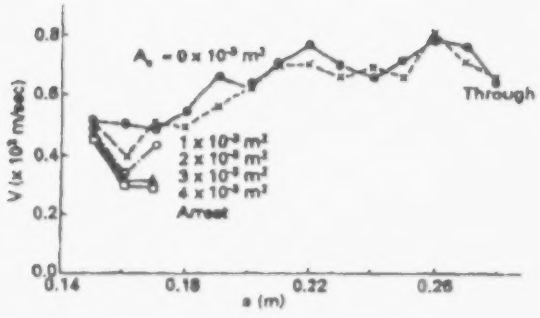

Figure 5-40 Crack propagation with different A_s (X_0 = 0.18 m) [14]

The influence of the stiffener position was then examined The variation of K_I with stiffener position is plotted in Figure 5-41 It can be seen that K_I increases as the stiffener is located farther from the centre of the crack, X_0 The value of K_I then became stable and equal to the unstiffened value if X_0 is greater than approximately 0 21 m I' is plotted against a in Figure 5-42 for various values of X_0 The crack did not propagate for the case X_0 = 0 15 m It can be seen from the figure that crack arrest occurred for the case of X_0 = 0 18 m I' was reduced when the crack tip was near the stiffener for the cases X_0 = 0 21 and 0 24 m and increased after the crack grew past the stiffener

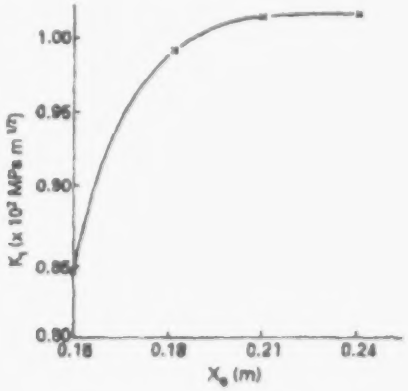

Figure 5-41 Static K_I variation with X_0 (A_s = 0.2 x 10^{-3} m^2) [14]

P516758.PDF [Page: 90 of 96]

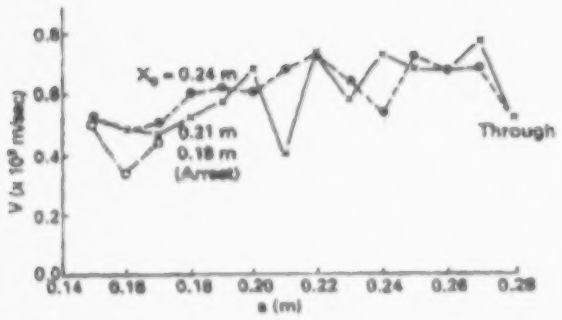

Figure 5-42 Crack propagation with different X_0 ($A_r = 0.2 \times 10^{-3}$ m^2) [14]

P516758.PDF [Page: 91 of 96]

6 Summary

Griffth's fracture criterion states that fracture can occur if the strain energy release rate of a body is greater than a critical value This critical value is the so-called crack resistance The fracture stress of a structure at a given crack size is called the residual strength When strain energy release rate is greater than the crack resistance, the surplus energy can be converted into kinetic energy for a growing crack The crack is arrested when all the kinetic energy is consumed In a stiffened structure, the crack tip stress intensity factor and the strain energy release rate is lowered at the vicinity of a stiffener as the stress in the stiffener and fastener increases The strain energy release rate can drop below the crack resistance of the structure to the point that crack arrest is possible At the same time the residual strength of the structure increases as the crack approaches the stiffener There are several parameters that affect the effectiveness of a stiffener They are the fastener spacing, stiffener spacing, and the relative stiffness parameter Similarly, the failure of the stiffener and the fasteners affect the overall effectiveness of a stiffened structure The behaviour of a stiffened structure can be modeled by several methods Some of these include the analytical method, finite element method, boundary element method, and the finite difference method These methods have been employed by various investigators to analyze a variety of cracked stiffened panel problems Their results were discussed in this report

P516758.PDF [Page: 92 of 96]

References

1 Anderson, T L , *Fracture Mechanics: Fundamentals and Applications* Second Edition, CPR Press, Inc , Florida, 1995

2 Broek, D , *Elementary Engineering Fracture Mechanics* Martinus Nijhoff Publishers, The Hague, 1983

3 Broek, D , *The Practical Use of Fracture Mechanics*, Kluwer Academic Publishers, The Netherlands, 1989

4 Hibbeler, R C , *Structural Analysis*, Third Edition, Prentice Hall, Upper Saddle River, New Jersey, 1997

5 Liu, Z H , Wang, Y H , Xie, D , and Ding, W , "Dynamic Fracture Analysis of Stiffened Panel by Finite Difference Method", *Computational Mechanics*, 1991, pp 915-920

6 Liu, A F , *Structural Life Assessment Methods*, ASM International, USA, 1998

7 Maiti, S K , and Sethuraman, R , "A Higher Order Element for Finite Element Analysis of Stiffened Panels Subjected to In-plane Loading and a Study on Efficient Arrangement of Doubly Bonded Strip Crack Stiffeners", *Engineering Fracture Mechanics*, Vol 41, No 3, 1992, pp 349-365

8 Nishimura, T , "Stress Intensity Factors of Multiple Cracked Sheet with Riveted Stiffeners", *Journal of Engineering Materials and Technology*, Vol 113, July 1991, pp 280-284

9 Rooke, D P , Acors, S , Fedelinski, P , "Dynamic Effects of Breaking Stiffeners in Cracked Structures", *Engineering Fracture Mechanics*, Vol 52, No 5, 1995, pp 811-820

10 Rushton, P A , *A Review of Fracture Mechanics, Fatigue, and Fatigue Crack Propagation* MASc Report, DalTech, 2000

11 Salgado, N K , and Aliabadi, M H., "The Application of the Dual Boundary Element Method to the Analysis of Cracked Stiffened Panels", *Engineering Fracture Mechanics*, Vol 54, No 1, 1996, pp 91-105

12 Sethuraman, R , and Maiti, S K , "Determination of Mixed Mode Stress Intensity Factors for a Crack-Stiffened Panel", *Engineering Fracture Mechanics*, Vol 33, No 3, 1989, pp 355-369

P516758.PDF [Page: 93 of 96]

13 Sethuraman, R , and Maiti, S K , "Finite Element Analysis of Doubly Bonded Crack-Stiffened Panels Under Mode I or Mode II Loading", *Engineering Fracture Mechanics*, Vol 34, No 2, 1989, pp 465-475

14 Wang, Y H , Liu, Z H , and Wang, J , "Dynamic Fracture Analysis of a Stiffened Panel with an Edge Crack", *Engineering Fracture Mechanics*, Vol 46, No 2, 1993 pp 329-338

PS16758.PDF [Page: 94 of 96]

UNCLASSIFIED
SECURITY CLASSIFICATION OF FORM
(highest classification of Title, Abstract, Keywords)

DOCUMENT CONTROL DATA

(Security classification of title, body of abstract and indexing annotation must be entered when the overall document is classified)

1 ORIGINATOR (the name and address of the organization preparing the document. Organizations for whom the document was prepared, e.g. Establishment sponsoring a contractor's report, or tasking agency, are entered in section 8.)

Department of Civil Engineering, Dalhousie University
PO Box 1000, Halifax, Nova Scotia, Canada, B3J 2X4

2 SECURITY CLASSIFICATION (overall security classification of the document including special warning terms if applicable)

UNCLASSIFIED

3 TITLE (the complete document title as indicated on the title page. Its classification should be indicated by the appropriate abbreviation (S,C,R or U) in parentheses after the title)

A Review of Literature: Experimental and Computational Investigation of Fatigue Crack Propagation in Stiffened Plates

4 AUTHORS (Last name, first name, middle initial. If military, show rank, e.g. Doe, Maj. John E.)

Yuen, Brian and Taheri, Farid

5 DATE OF PUBLICATION (month and year of publication of document)

September 2001

6a NO. OF PAGES (total containing information. Include Annexes, Appendices, etc.)

85

6b NO. OF REFS (total cited in document)

14

7 DESCRIPTIVE NOTES (the category of the document, e.g. technical report, technical note or memorandum. If appropriate, enter the type of report, e.g. interim, progress, summary, annual or final. Give the inclusive dates when a specific reporting period is covered)

CONTRACTOR REPORT

8 SPONSORING ACTIVITY (the name of the department project office or laboratory sponsoring the research and development. Include address)

Defence Research Establishment Atlantic
PO Box 1012
Dartmouth, NS, Canada B2Y 3Z7

9a PROJECT OR GRANT NO. (if appropriate, the applicable research and development project or grant number under which the document was written. Please specify whether project or grant)

Project 1gc11

9b CONTRACT NO. (if appropriate, the applicable number under which the document was written)

W7707-008441/001/HAL

10a ORIGINATOR'S DOCUMENT NUMBER (the official document number by which the document is identified by the originating activity. This number must be unique to this document.)

none

10b OTHER DOCUMENT NOs. (Any other numbers which may be assigned this document either by the originator or by the sponsor.)

DREA CR 2001-141

11 DOCUMENT AVAILABILITY (any limitations on further dissemination of the document, other than those imposed by security classification)

(X) Unlimited distribution
( ) Defence departments and defence contractors; further distribution only as approved
( ) Defence departments and Canadian defence contractors; further distribution only as approved
( ) Government departments and agencies; further distribution only as approved
( ) Defence departments; further distribution only as approved
( ) Other (please specify):

12 DOCUMENT ANNOUNCEMENT (any limitation to the bibliographic announcement of this document. This will normally correspond to the Document Availability (11). However, where further distribution (beyond the audience specified in (11) is possible, a wider announcement audience may be selected)

Unlimited

UNCLASSIFIED
SECURITY CLASSIFICATION OF FORM

PSTC/58.PDF [Page: 93 of 96]

UNCLASSIFIED
SECURITY CLASSIFICATION OF FORM

13. ABSTRACT (a brief and factual summary of the document. It may also appear elsewhere in the body of the document itself. It is highly desirable that the abstract of classified documents be unclassified. Each paragraph of the abstract shall begin with an indication of the security classification of the information in the paragraph (unless the document itself is unclassified) represented as (S), (C), (R), or (U). It is not necessary to include here abstracts in both official languages unless the text is bilingual)

This report is a review of the subject of fracture mechanics focusing mainly on its application on stiffened sheet structures. It is written for readers who have some basic knowledge of fracture mechanics in a general sense but are interested in learning more on this specific and complex aspect of the subject. This report has six chapters. Chapter one is an introduction that focuses on the application of stiffened sheet structures. Chapter two reviews the fracture mechanics concepts of strain energy release rate, stress intensity factor, crack resistance and residual strength. Chapter three presents the general theories behind dynamic fracture mechanics and the crack arrest process. Chapter four applies the concepts and theories from Chapter two and three to stiffened sheet structures. Factors that can be used in designing these structures and various parameters that affect their performance are described in this chapter. The graphical representations of the crack arrest process in these structures are also presented in this chapter. Chapter five discusses several methods for analyzing and modeling stiffened sheet structures. In particular the analytical method, the finite element method, the boundary element method, and the finite difference method are presented. Results from several investigators demonstrate the effectiveness of each of these methods. Chapter six contains the concluding remarks on this report.

14. KEYWORDS, DESCRIPTORS or IDENTIFIERS (technically meaningful terms or short phrases that characterize a document and could be helpful in cataloguing the document. They should be selected so that no security classification is required. Identifiers, such as equipment model designation, trade name, military project code name, geographic location may also be included. If possible keywords should be selected from a published thesaurus, e.g. Thesaurus of Engineering and Scientific Terms (TEST) and that thesaurus-identified. If it not possible to select indexing terms which are Unclassified, the classification of each should be indicated as with the title)

Ship
Structures
Fracture
Fatigue
Stiffener

UNCLASSIFIED
SECURITY CLASSIFICATION OF FORM

P516758.PDF [Page: 96 of 96]

Defence R&D Canada
is the national authority for providing
Science and Technology (S&T) leadership
in the advancement and maintenance
of Canada's defence capabilities.

R et D pour la défense Canada
est responsable, au niveau national, pour
les sciences et la technologie (S et T)
au service de l'avancement et du maintien des
capacités de défense du Canada.

#516758
CA020089

DEFENCE R&D DÉFENSE

www.drdc-rddc.dnd.ca